HEP'97 #419
Submitted to Pa 5, 7, 11
Pl 7, 15, 19

DELPHI 97-106 CONF 88
20 July, 1997

Measurement of the partial decay width $R_b^0 = \Gamma_{b\bar{b}}/\Gamma_{had}$ with the DELPHI detector at LEP

Preliminary

DELPHI Collaboration

G.J.Barker[a], G.Borisov[b,1], C.De la Vaissiere[c], R.McNulty[a], C.Mariotti[a,2], F.Martinez-Vidal[d], K.Mönig[a], A.M.Normand[e]

a CERN, CH=1211 Geneva 23, Switzerland
b CEA Saclay, DSM/DAPNIA, France
c LPNHE, Universite' Paris VI et VII, France
d IFIC, Universitat de Valencia, Spain
e University of Liverpool, England
1 *On leave of absence from IHEP, Protvino, Russian Federation*
2 *On leave of absence from INFN, Italy.*

Abstract

The partial decay width of the Z to $b\bar{b}$ quark pairs has been measured by the DELPHI detector at LEP using data taken with the upgraded microvertex detector installed in spring 1994. B-hadrons, containing b-quarks, were tagged by several methods using either tracks with large impact parameters to the primary vertex complemented by event shape variables or reconstructed inclusive secondary vertices.

Combining these methods in a Multivariate Analysis the value:

$$\frac{\Gamma_{b\bar{b}}}{\Gamma_{had}} = 0.21660 \pm 0.00082(stat.) \pm 0.00088(syst.)$$

was found, where the $c\bar{c}$ production fraction was fixed to its Standard Model value.

Paper submitted to the HEP'97 Conference
Jerusalem, August 19-26

1 Introduction

The relative decay width of the Z into B-hadrons, $R_b^0 = \frac{\Gamma_{b\bar{b}}}{\Gamma_{had}}$, has been measured with very high precision at LEP and SLD [1, 2, 3, 4, 5, 6]. Experimentally, R_b^0 can be obtained with only very small corrections from the ratio of cross-sections $R_b = \sigma(e^+e^- \to b\bar{b})/\sigma(e^+e^- \to$ hadrons). The average value of R_b^0 [7] disagrees by about two standard deviations with the prediction of the Standard Model. To resolve the question of whether this deviation is real, new analyses including more data are needed. This paper presents three measurements of R_b using about 2.1 million hadronic events taken in 1994 and 1995 with the DELPHI detector at LEP.

All three analyses compare single and double tag rates, from which R_b can be measured together with the b-tagging efficiency. Systematic errors due to the charm background and to hemisphere correlations have been considerably reduced with respect to previous analyses [3] using new variables to identify the b-quarks and different algorithms to reconstruct the primary vertex.

The data collected in 1994 and 1995 have been reprocessed with a new reconstruction program that greatly enhances the tracking efficiency and resolution with respect to the previous one. The data from earlier years (1991–1993) are still under reprocessing, and so are not included in the current results.

2 The DELPHI Detector

The DELPHI detector and its performance have been described in detail elsewhere [8, 9]. Only the details most relevant to this analysis are mentioned here and particular care is given to the new microvertex detector, installed in spring 1994, that allowed high values of purity and efficiency in the identification of the b quarks to be reached.

In the barrel region, the charged particle tracks are measured by a set of cylindrical tracking detectors whose axes are parallel to the 1.2 T solenoidal magnetic field and to the beam direction.

The innermost one is the microvertex detector (VD), which is located between the LEP beam pipe and the Inner Detector (ID) [10, 11]. To increase the performance of the detector in tracking and especially in the identification of B-hadrons, in 1994 the DELPHI VD [10] was upgraded to become a three-dimensional detector [11]. It consists of three concentric layers of silicon microstrip detectors at radii of 6.3, 9 and 11 cm from the beam line, respectively called the closer, inner and outer layers. The microstrip detectors of the closer and outer layers provide hits in both the $R\phi$ and the Rz planes, while for the inner layer only the $R\phi$ coordinate is measured. For polar angles of $44^\circ \leq \theta \leq 136^\circ$ a track crosses all three silicon layers of the VD. The closer layer covers the polar region between 25° and 155°.

The measured intrinsic resolution is about 8 μm for the $R\phi$ coordinate, while for Rz it depends on the incident polar angle of the track and reaches about 9 μm for tracks perpendicular to the modules. For charged tracks with hits in all three $R\phi$ VD layers the impact parameter resolution is $\sigma^2_{R\phi} = ((61/(P\sin^{3/2}\theta))^2 + 20^2)\mu m^2$ and for tracks with hits in both Rz layers and with $\theta \approx 90^\circ$, $\sigma^2_{Rz} = ((67/(P\sin^{5/2}\theta))^2 + 33^2)\mu m^2$.

The time projection chamber (TPC) is the main tracking device and is a cylinder with a length of 3 m, an inner radius of 30 cm and an outer radius of 122 cm. Between polar

angles, θ, of 39° and 141° with respect to the beam direction, tracks are reconstructed using up to 16 space points. Outside this region (21° to 39° and 141° to 159°), tracks can be reconstructed using at least 4 space points.

Additional precise $R\phi$ measurements, in the plane perpendicular to the magnetic field, are provided at larger and smaller radii by the Outer and Inner detectors respectively. The Outer Detector (OD) has five layers of drift cells at radii between 198 and 206 cm and covers polar angles from 42° to 138°. The Inner Detector (ID) is a cylindrical drift chamber having inner radius of 12 cm and outer radius of 28 cm and covers polar angles between 29° and 151° . It contains a jet chamber section providing 24 $R\phi$ coordinates, surrounded by five layers of proportional chambers giving both $R\phi$ and longitudinal z coordinates.

The barrel electromagnetic calorimeter (HPC) covers polar angles between 42° and 138°. It is a gas-sampling device which provides complete three-dimensional charge information in the same way as a time projection chamber. The excellent granularity allows good separation between close particles in three dimensions and hence good electron identification even inside jets.

In the forward region the tracking is complemented by two sets of planar drift chambers (FCA and FCB), at distances of $\pm$165 cm and $\pm$275 cm from the interaction point. A lead glass calorimeter (EMF) is used to reconstruct electromagnetic energy in the forward region.

Muon identification in the barrel region is based on a set of muon chambers (MUB), covering polar angles between 53° and 127°. In the forward region the muon identification is done using two sets of planar drift chambers (MUF) covering the angular region between 11° and 45°.

3 Event Selection

The criteria to select charged tracks and to identify hadronic Z decays were identical to those described in [3]. Charged particles were accepted if:

- their polar angle was between 20° and 160°,
- their track length was larger than 30 cm,
- their impact parameter relative to the interaction point was less than 2.5 cm in the plane perpendicular to the beam direction and less than 10 cm along the beam direction,
- their momentum was larger than 200 MeV/c with relative error less than 100%.

Neutral particles detected in the HPC were required to have measured energy larger than 700 MeV and those detected in the EMF greater than 400 MeV.

Events were then selected by requiring:

- at least 6 reconstructed charged particles,
- the summed energy of the charged particles had to be larger than 15% of the centre of mass energy, with at least 3% of it in each of the forward and backward hemispheres with respect to the beam axis.

The efficiency to find hadronic Z decays with these cuts was about 95% (94%) for the 1994 (1995) data sample with only a very small bias towards a specific flavour, and all backgrounds were below 0.1%.

About 1400000 hadronic Z decays were selected from the 1994 data sample and 700000 from 1995. The ratio of the cross-section $Z \to b\bar{b}$ to the total hadronic cross-section varies very little at centre of mass energies close to the Z mass. Thus no selection on the centre of mass energy was made in 1995. However the validity of this assumption has been tested in [3] and in section 5. A sample about twice the data statistics of $Z \to q\bar{q}$ events was simulated using the Lund parton shower Monte Carlo JETSET 7.3 [12] (with parameters optimized by DELPHI) and the DELPHI detector simulation [9]. In addition dedicated samples of $Z \to b\bar{b}$ events were generated. The simulated events were passed through the same analysis chain as the real ones.

4 The Combined Impact Parameter Analysis

4.1 The method

Events are divided into hemispheres using the plane perpendicular to the thrust axis. If R_H is the fraction of hemispheres tagged as b and R_E is the fraction of events in which both hemispheres are tagged, R_b can be extracted by comparison of the single and double tag rates:

$$\begin{aligned} R_H &= R_b \cdot \epsilon_b + R_c \cdot \epsilon_c + (1 - R_b - R_c) \cdot \epsilon_{uds} \\ R_E &= R_b \cdot \epsilon_b^2 \cdot (1 + \rho) + R_c \cdot \epsilon_c^2 + (1 - R_b - R_c) \cdot \epsilon_{uds}^2, \end{aligned} \tag{1}$$

where ϵ_q is the efficiency to tag a hemisphere originating from a primary quark q (=b, c, uds) and the coefficient ρ accounts for hemisphere correlations in the tagging efficiencies for b-quarks. For the other quark species these correlation factors can safely be neglected due to the very high b purity reached. If ρ, ϵ_c and ϵ_{uds} are calculated from the simulation and R_c is imposed from other measurements or from the Standard Model, R_b and ϵ_b can be measured simultaneously from the data. A good knowledge of the details of B-hadron decays is thus not required.

A new b-tagging algorithm was used. The main ingredient was the measurement of the track impact parameters. However it was complemented by additional information like the invariant mass and the energy of particles fitted to a secondary vertex. Where to cut in this variable is arbitrary and the cut chosen for the results was that which minimized the total error. Results are given as a function of the b purity and b efficiency of the data sample.

The two contributions to the systematic error are the background efficiencies and the hemisphere correlation coefficient ρ. The former can be substantially reduced using the purer tag. The second source is the correlation between the two hemispheres in the event. From the previous analysis [3], it was estimated that the major contribution to this came from the common primary vertex. The correlation can be substantially reduced whenever a separate primary vertex is computed for each hemisphere (first used in [3]). The remaining correlation is discussed in section 4.4.

As the VD is essential for the measurement of the impact parameters in both the $R\phi$ and the Rz planes, the method was limited to events that have most of the tracks inside the acceptance of the VD. For this reason a cut of $|\cos\theta_{thrust}| < 0.65$ was applied.

For the extraction of R_b with such a method, a good description of the data by the simulation for the $udsc$-quarks is required. For this reason a fine tuning of the $R\phi$ and Rz impact parameter distributions in the simulation was developed and applied [13]. This led to substantially smaller uncertainties due to the understanding of the detector resolution.

4.2 Tagging technique

B-hadrons are significantly different from all other particles. They have a large mass, a long lifetime and a high decay multiplicity, they take more energy than light hadrons from the initial quark, etc. However in previous DELPHI measurements of R_b, only their long lifetime and the high decay multiplicity were used for the tagging [3]. In this paper we describe a method of b-tagging which combines all these differences of the B-hadron with respect to other particles into a single variable. This method has a strong mathematical background which guarantees the optimal way of combination in the case of uncorrelated discriminating variables. Application of this method gives a significant improvement of the b-tagging efficiency with respect to the lifetime tag used previously.

In this method which is described in detail in [14] all discriminating variables are defined for jets (using JADE with y_{min}=0.01) with reconstructed secondary vertices. The jets without reconstructed secondary vertices are not considered. Such a condition allows the properties specific to B-hadrons to be used for the tagging and allows the separation of their decay products from the particles coming from b-quark hadronization. In addition, the requirement of jets with reconstructed secondary vertices is a good selection by itself as it removes a significant part of the background. The purity of B-hadrons in jets with secondary vertices is about 85% with a selection efficiency of almost 50%.

The reconstructed secondary vertex is required to contain at least 2 tracks not compatible with the primary vertex and to have $L/\sigma_L > 4$, where L is the distance from the primary to the secondary vertex and σ_L is its error. Each track included in the secondary vertex should have at least one measurement in the VD and at least 2 tracks should have measurements in both the $R-\phi$ and the $R-z$ planes of the VD.

The description of the discriminating variables is as follows.

The jet lifetime probability, P_j^+, is constructed from the positively signed impact parameters of the tracks included in a jet and corresponds to the probability of a given group of tracks being compatible with the primary vertex [15, 16]. For jets with B-hadrons, this probability is very small due to the significant impact parameters of tracks from B-decays. However, jets with c-quarks can also have low values of P_j^+ because of the non-zero lifetime of D-mesons, which limits the performance of the lifetime tag. The distribution of $-\log_{10}(P_j^+)$ for different quark flavours is shown in figure 1a.

The distribution of **the effective mass of particles included in the secondary vertex**, M_s, is shown in figure 1b. The mass of the secondary vertex for c-jets is limited by the mass of D-mesons and above $M_s = 1.8\,\mathrm{GeV}/c^2$ the number of vertices in c-jets decreases sharply, while that in b-jets extends up to $5\,\mathrm{GeV}/c^2$.

The distribution of **the rapidity of tracks included in the secondary vertex with respect to the jet direction**, R_s^{tr}, is shown in figure 1c. Although a B-hadron has on average higher energy than a D-meson from a c-jet, the rapidity of particles from a B-decay is on average less than that from a c-quark decay. This is explained by the higher mass of the B-hadron and the larger multiplicity of its decays. The secondary vertices in light quark jets are induced mainly by wrongly measured tracks. The wrong

measurements occur due to multiple scattering in the detector, interaction in the material, etc so that tracks included in the secondary vertices of light quark jets are usually soft and their rapidity distribution is shifted to lower values.

The distribution of **the fraction of the charged energy of a jet included in the secondary vertex**, X_s^{ch}, for different quark types is shown in figure 1d. In the case of B-hadrons, when almost all particles included in the secondary vertex come from the B-decay, the distribution of X_s^{ch} is determined by the fragmentation function $f(b \to B)$. The same is valid for c-quark jets where the distribution of X_s^{ch} is determined by $f(c \to D)$, which is softer than $f(b \to B)$. In light quark jets, the energy of the secondary vertex is much less than that in b-quark jets, as explained above.

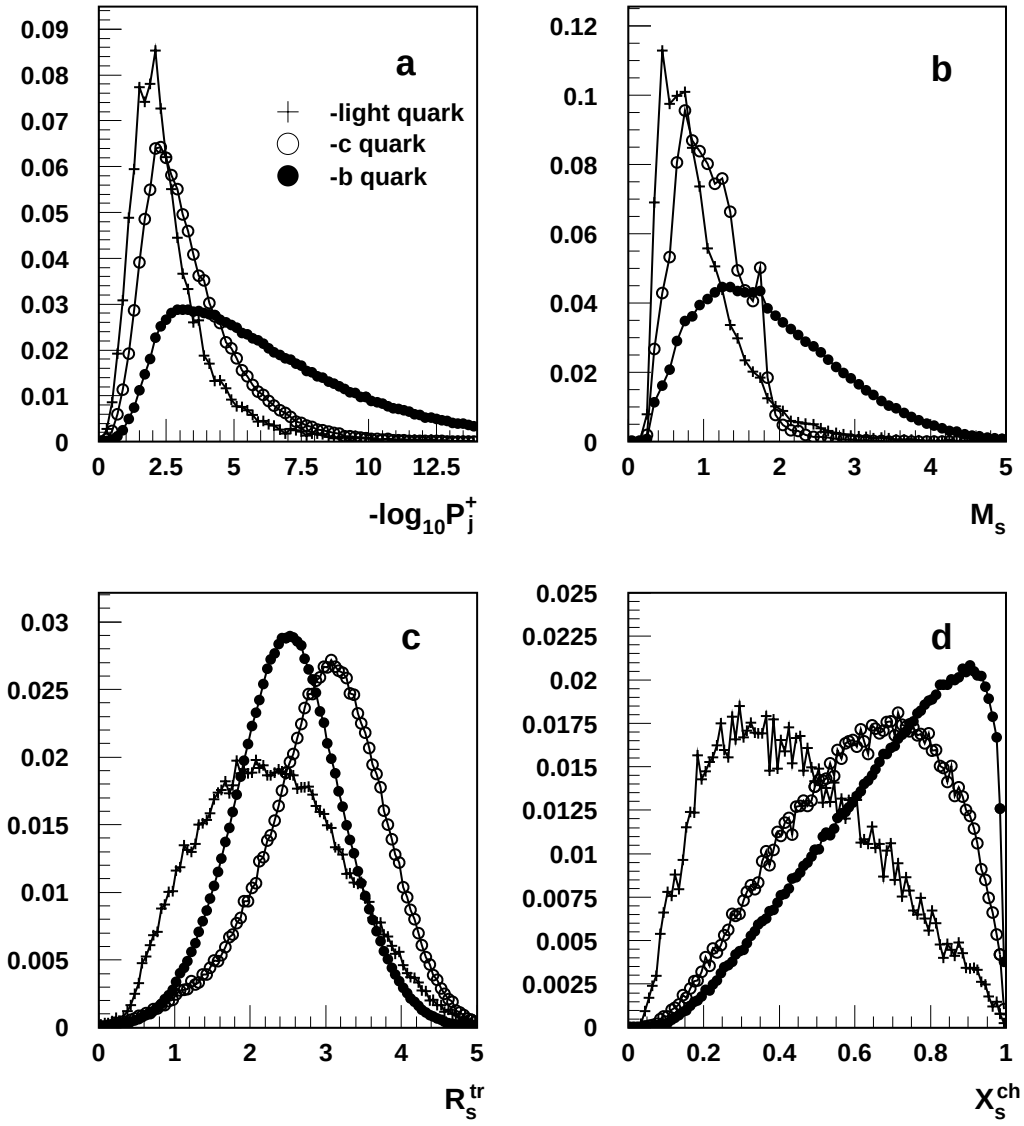

Figure 1: Distributions of discriminating variables used in the tagging.

For the combination of discriminating variables we define the following quantity:

$$y = n_c \cdot \prod \frac{f_i^c(x_i)}{f_i^b(x_i)} + n_q \cdot \prod \frac{f_i^q(x_i)}{f_i^b(x_i)} = n_c \cdot \prod y_i^c + n_q \cdot \prod y_i^q, \qquad (2)$$

where n_c, n_q is the normalized number of jets with a reconstructed secondary vertex in $c\bar{c}$ and $q\bar{q}$ events respectively ($n_c + n_q = 1$) and $f_i^q(x_i)$, $f_i^c(x_i)$, $f_i^b(x_i)$ are probability density functions of the variable x_i in uds-, c- and b-quark jets.

The products in (2) run over all tagging variables of a given jet. The variable R_s^{tr} is defined for each particle included in the secondary vertex and so the corresponding ratio of probabilities for each particle enters in equation (2). For the transformations $y_i^c(x_i) = f_i^c(x_i)/f_i^b(x_i)$ and $y_i^q(x_i) = f_i^q(x_i)/f_i^b(x_i)$ we use smooth functions which are obtained from a fit of the ratios of corresponding distributions. The jet is tagged as containing a b-quark if $y < y_0$, where the value y_0 can be varied to select the desired purity or efficiency of tagging.

Figure 2 shows the tagging efficiency versus purity of the selected sample for different combinations of discriminating variables. It can be seen that the addition of each new variable improves the tagging performance.

The combined tagging in comparison with the simple lifetime tag P_j^+ suppresses the content of background by more than 3 times for a b-tagging efficiency of 30% and about 6 times for a b-tagging efficiency of 20%. A very pure b sample with purity more than 99.5% can be obtained with the sizable b-efficiency 20%.

All distributions for this tagging method are taken from simulation, so that a check of their agreement with data is important for its successful application. For a measurement of R_b, only the agreement of background distributions should be verified since the efficiency of b-quark tagging is taken from data.

The high purity of the tagged sample allows the extraction from data of the distributions of the discriminating variables for background and the comparison of them with those used in the simulation. B-hadrons in one hemisphere are tagged with a high purity of about 99% to give a clean and almost uncontaminated sample of B-hadrons in the opposite hemisphere. The distributions of the discriminating variables in such hemispheres can be subtracted after appropriate normalization from the corresponding distributions in the untagged sample of jets with secondary vertices. These contain large contamination from other quark flavours and thus the distributions of discriminating variables for background can be obtained.

The comparison of these distributions in data and in simulation is shown in figure 3. Good agreement in the background description for all variables used in the tagging can be seen. Finally, figure 4 shows the comparison of distributions of the combined tagging variable $-\log_{10} y$, where y is defined by (2).

4.3 Light quark efficiencies

The analysis was performed at many different values of the b efficiency and b purity. The minimum total error in the 1994 data analysis was obtained for $\epsilon_b = 32.4\%$, i.e. for a cut on the variable $-\log_{10} y \geq 1$.

At this chosen working point the tagging efficiencies for uds and c quarks were estimated using the simulation to be

$$\epsilon_{uds} \quad = \quad 0.00063 \pm 0.00013 \qquad (3)$$

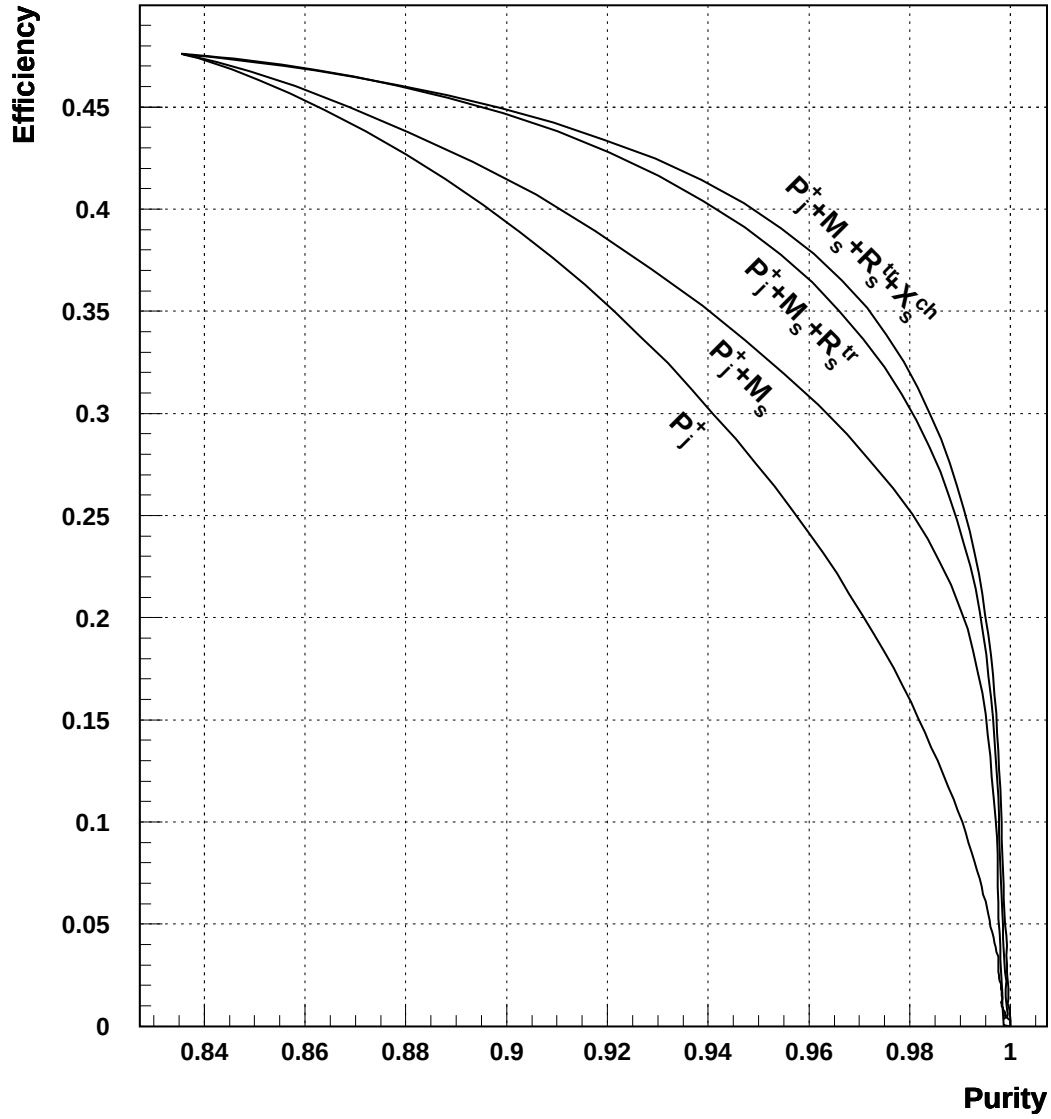

Figure 2: b-tagging efficiency versus purity of selected sample of jets with reconstructed secondary vertices for different compositions of discriminating variables.

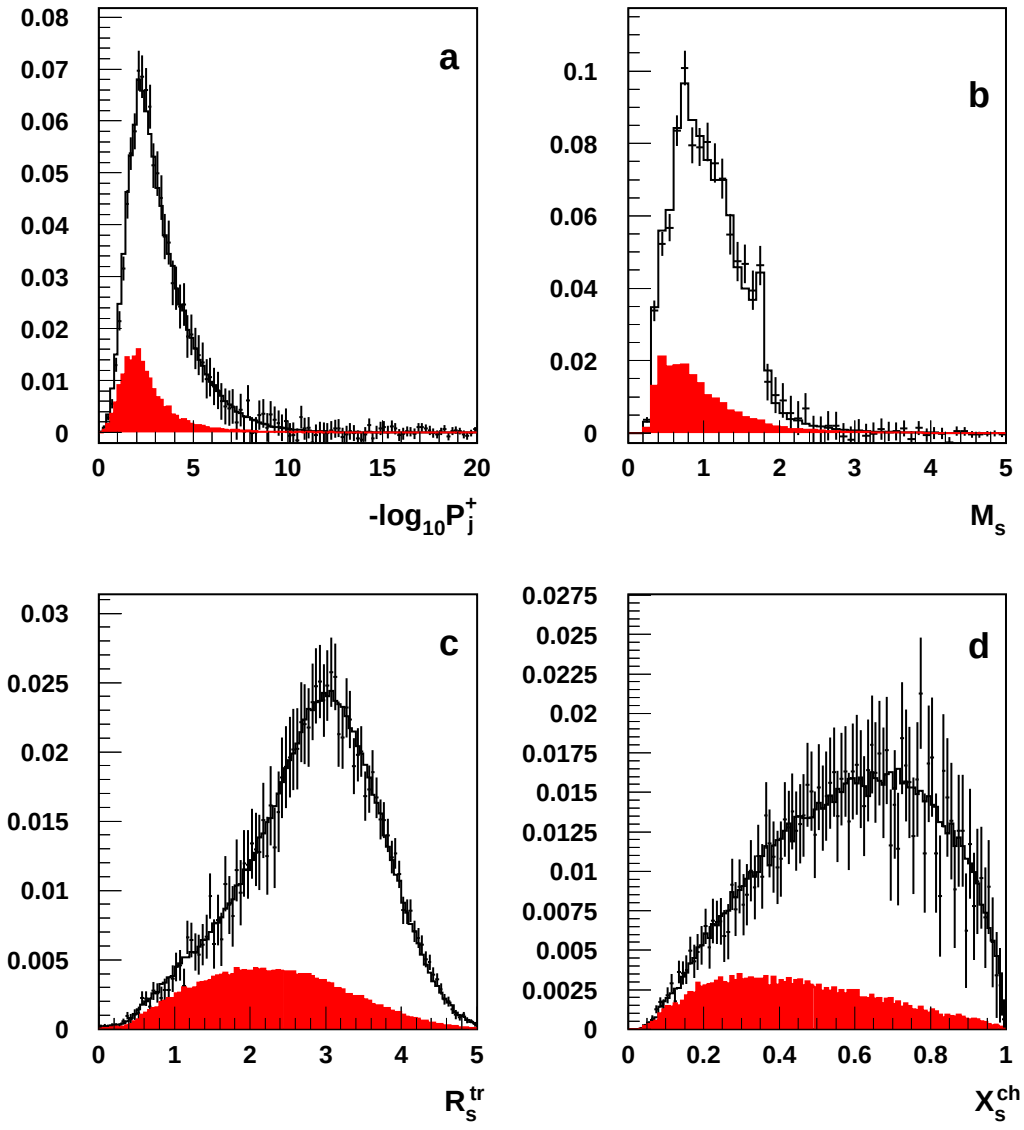

Figure 3: Distribution of discriminating variables for background (u, d, s, c) jets. The points with errors are from the data and histogram is the simulation prediction. The contribution of light quark jets is shown as the filled histograms.

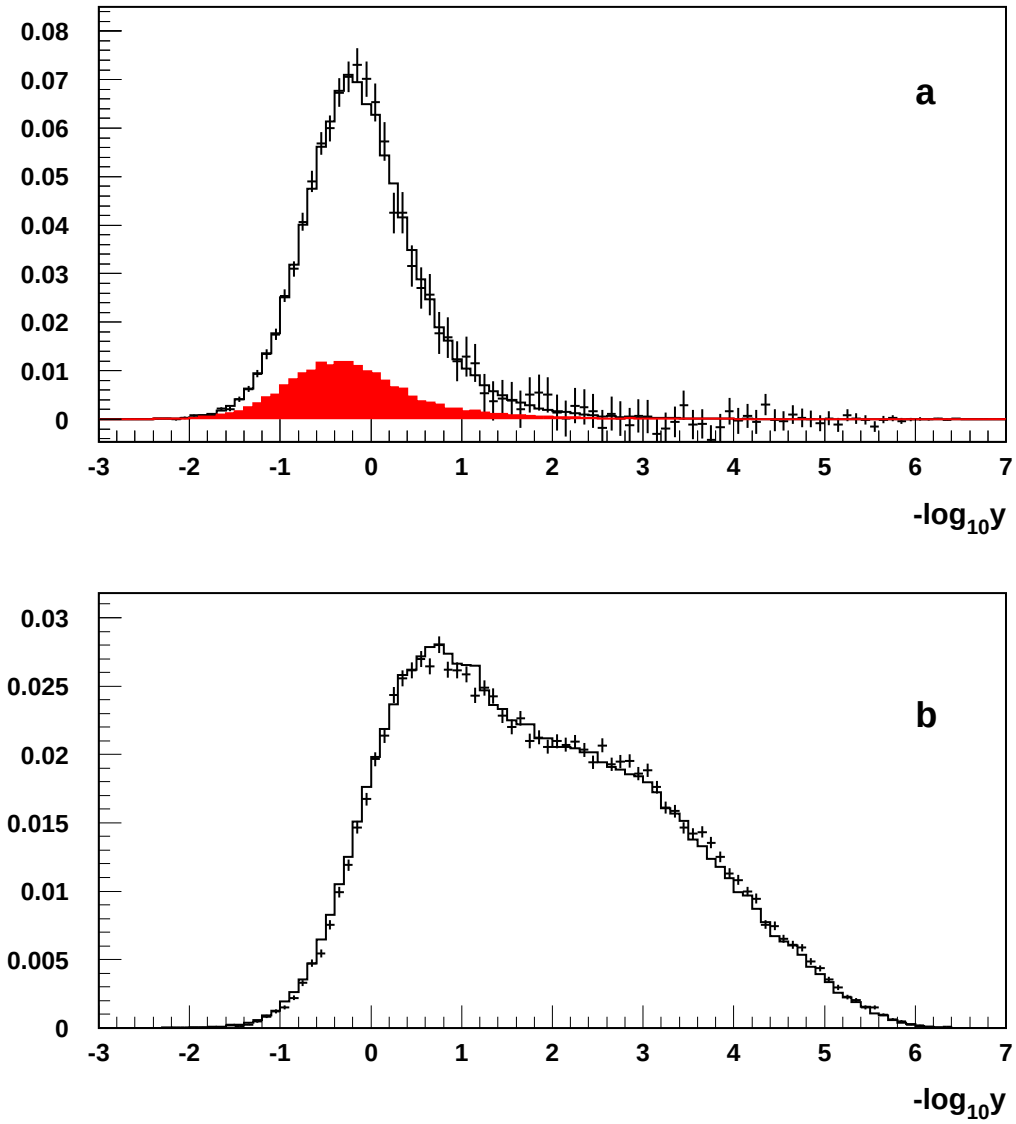

Figure 4: Distribution of the combined tagging variable $-\log_{10} y$ for (a) background (u, d, s, c) jets and (b) jets with b-quarks. The points with errors are from the data and the histogram is the simulation prediction. The contribution of light quark jets is shown as the filled histogram in the upper figure.

$$\epsilon_c \;=\; 0.00590 \pm 0.00048.$$

The breakdown of the errors is given in table 1. For all physics assumptions the recommendations of the LEPHF group [17] have been followed.

To estimate the uncertainty on ϵ_{uds} and ϵ_c due to detector effects four tests were carried out.

- To estimate the effect of the resolution, the simulation was rerun with a tuning [13] that described the data much worse than the default one (about 4% relative difference in the light and charm quark efficiencies).
- Another test for the effect of the detector resolution for ϵ_c was to use the calibration file for data in the simulation. For ϵ_c this method was preferred since it directly tests the difference between the data and the simulation used. However it gave results consistent with the other method. For ϵ_{uds} it cannot be used, as it artificially modifies the tagging rate due to statistical fluctuations.
- To estimate the effect of correlations between tracks included in the probability calculation, the difference in tagging rate between data and simulation using tracks with negative impact parameters was taken as the uncertainty on ϵ_{uds}.
- The track efficiency in the simulation was varied by the amount of the residual difference between the data and the Monte Carlo.

The errors obtained with the first, third and fourth tests were added in quadrature to obtain the final detector uncertainty on ϵ_{uds}. For ϵ_c only the second and fourth tests were used.

4.4 Hemisphere correlations

In the extraction of R_b, one has to correct for the fact that the two hemispheres in an event are not completely uncorrelated. Due to the high purity, this effect can safely be neglected for non-b events. For b events a correlation coefficient for the 1994 data analysis $\rho = \frac{\epsilon_b^{(d)}}{\epsilon_b^2} - 1$ was introduced which was estimated from the simulation to be

$$\rho = 0.0106 \pm 0.0030 \tag{4}$$

at the chosen working point of $-\log_{10} y \geq 1$.

Two main effects are responsible for ρ not being equal to zero.

- Angular effects: the particles in an event are typically nearly back to back. This leads to a positive correlation due to the polar angle. The multiple scattering contribution to the VD resolution increases with decreasing polar angle and close to the end of the VD some tracks get lost outside its acceptance. There are also some minor effects connected with the azimuthal angle. Due to the flatness of the beamspot at LEP the resolution is better for horizontal than for vertical jets and due to inefficient or badly aligned modules the detector is not completely homogeneous.

Source of systematics	Range	$\Delta\epsilon_{uds} \times 10^5$	$\Delta\epsilon_c \times 10^4$
MC statistics		± 2.3	± 1.1
Detector resolution		± 3.3	± 1.3
Detector efficiency		± 1.0	± 0.8
K^0	Tuned JETSET$\pm$10%	± 0.8	
Hyperons	Tuned JETSET$\pm$10%	± 0.1	
Photon conversions	$\pm$50%	± 0.4	
Gluon splitting $g \to b\bar{b}$	$(0.31 \pm 0.11)\%$[1]	± 10.9	± 1.2
Gluon splitting $g \to c\bar{c}$	$(2.38 \pm 0.48)\%$[1]	± 2.7	± 0.3
D^+ fraction in $c\bar{c}$ events	0.223 ± 0.028[1]		± 1.8
D_s fraction in $c\bar{c}$ events	0.102 ± 0.037[1]		∓ 0.5
c-bar. fraction in $c\bar{c}$ events	0.065 ± 0.029[1]		∓ 1.3
D decay multiplicity	see [17]		± 1.3
$BR(D \to K^0 X)$	0.46 ± 0.06		± 3.0
D^0 lifetime	0.415 ± 0.004 ps		± 0.3
D^+ lifetime	1.057 ± 0.015 ps		± 0.4
D_s lifetime	0.447 ± 0.017 ps		± 0.2
Λ_c lifetime	0.206 ± 0.012 ps		± 0.0
$\langle x_E(c) \rangle$	0.484 ± 0.008		± 0.5
Total		± 13.2	± 4.8

Table 1: Systematic errors on the light and charm quark efficiencies.
[1]: Correlation between these sources are taken into account

- QCD effects: the b-tagging efficiency rises with the momentum of the B-hadrons. Gluons emitted at large angles with respect to the quarks affect the energy of both quarks, leading to a positive correlation. In about 2% of the events both b quarks are boosted into the same hemisphere, recoiling against a hard gluon. This leads to a negative correlation.

To obtain the systematic error on the correlation estimate from the simulation, the fraction of tagged events was measured as a function of the relevant variable both in data and in simulation. From this, the correlation due to that single variable was calculated. This procedure uses the fact that the value of the test variable is correlated between the hemispheres, e.g. if one hemisphere has a cosine of its polar angle at z the other one has it at $-z$. The larger of either a) the difference between the data and simulation measurements or b) the statistical error on this difference was taken as the error estimate for this correlation source. For the angular variables all events have been used. Due to the high purity of the tag and because the initial angular distributions are identical for b and light quark events no bias was introduced. It was, however, verified that the conclusions did not change if a b-tag was required in the hemisphere opposite to the tested one.

To test the correlation due to QCD effects, all events were forced to three jets and the jet momenta were recalculated using energy-momentum conservation. The momentum of the fastest jet (p_{jet}) was then defined as the test variable with the convention that it was counted positive in the one-jet hemisphere and negative in the two-jet hemisphere. Since the p_{jet} distribution is different for b and $udsc$ events, a b-tag was required in the opposite hemisphere to avoid an artificial bias. As an additional complication, the two sources for QCD correlations act differently on the p_{jet} distribution. If the two b quarks are one in each hemisphere, the one-jet hemisphere represents the faster and thus better tagged b. If the two b quarks are boosted into the same hemisphere, the one-jet side contains only a gluon. For that reason the one-jet hemisphere was only used if it passed a soft b-tag. On the two-jet side, a soft b-tag cannot be applied since this changes drastically the ratio of events with a fast b and a soft gluon and vice versa.

Figure 5 shows the correlations obtained with this procedure in data and simulation. Also shown is the correlation obtained from an unbiased sample of $b\bar{b}$ events without events that have both b quarks in one hemisphere. The systematic error induced by events with both b quarks in one hemisphere was tested by varying their amount in simulation by 30%.

Some additional physics systematics like B-lifetimes, decay multiplicities and fragmentation were also tested by reweighting the simulation. The B hadron decay multiplicity was recently measured [18] and found to be consistent with the simulation input value. Consequently the simulation was not reweighted for this. To be conservative the error on this value was taken from [17]. However due to the use of separate hemisphere primary vertices, the effects of these additional physics systematics were found to be extremely small. The uncertainties on ρ are summarized in table 2.

4.5 Results

1352913 hadronic Z decays were selected in 1994, of which 818639 passed the $|\cos\theta_{thrust}|$ cut. Of these, 118192 single hemispheres were tagged and 18996 events were double tagged for $-\log_{10} y \geq 1$. The bias towards b events in the event selection was found to be small,

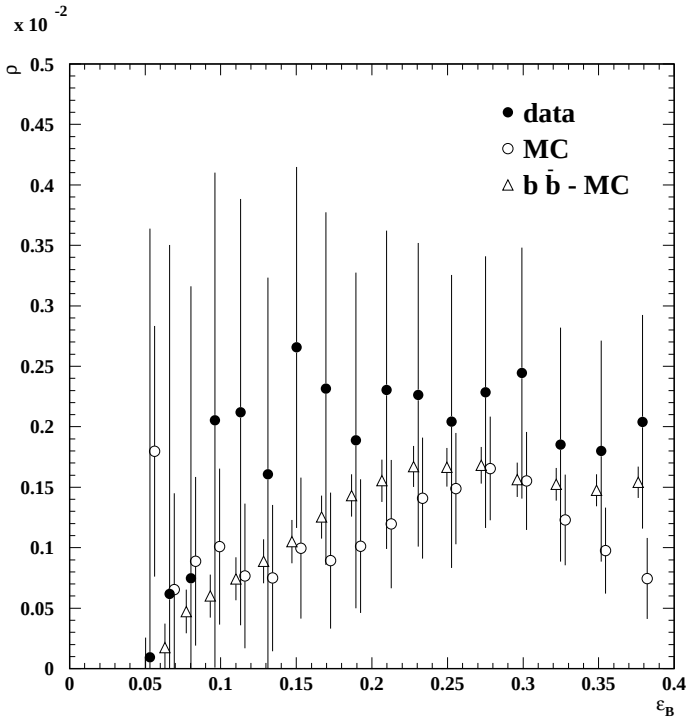

Figure 5: Hemisphere correlation due to gluon radiation as a function of the b-tagging efficiency. The closed and open circles show data and simulation respectively, selected as described in the text. The open triangles show an unbiased sample of simulated $b\bar{b}$ events without events that have two b quarks in one hemisphere.

Source of systematics	Range	$\Delta\rho \times 10^3$
MC statistics		± 2.3
angular effects		± 1.2
gluon radiation		± 1.0
2 b quarks in one hemisphere	$\pm 30\%$	± 0.3
B decay multiplicity		± 1.0
B lifetimes		± 0.2
B fragmentation		± 0.1
total		± 3.0

Table 2: Systematic errors on hemisphere correlations.

$(1.60 \pm 0.14) \cdot 10^{-3}$, and was corrected for. Using the above values of the efficiencies and the correlation, with their errors, the measured value of R_b is:

$$R_b = 0.21697 \pm 0.00119(stat.) \pm 0.00096(syst.) - 0.033 \times (R_c - 0.172). \quad (5)$$

Correcting for photon exchange yields:

$$R_b^0 = 0.21717 \pm 0.00119(stat.) \pm 0.00096(syst.) - 0.033 \times (R_c - 0.172). \quad (6)$$

The b hemisphere tagging efficiency was found to be $\epsilon_b = 0.3243 \pm 0.0018$, compared to $\epsilon_b(MC) = 0.314$ obtained from the simulation. In figure 6 the ratio of b-tagging efficiency in real data and in simulation is given as a function of the b efficiency. The real data were about 3% more efficient than simulation.

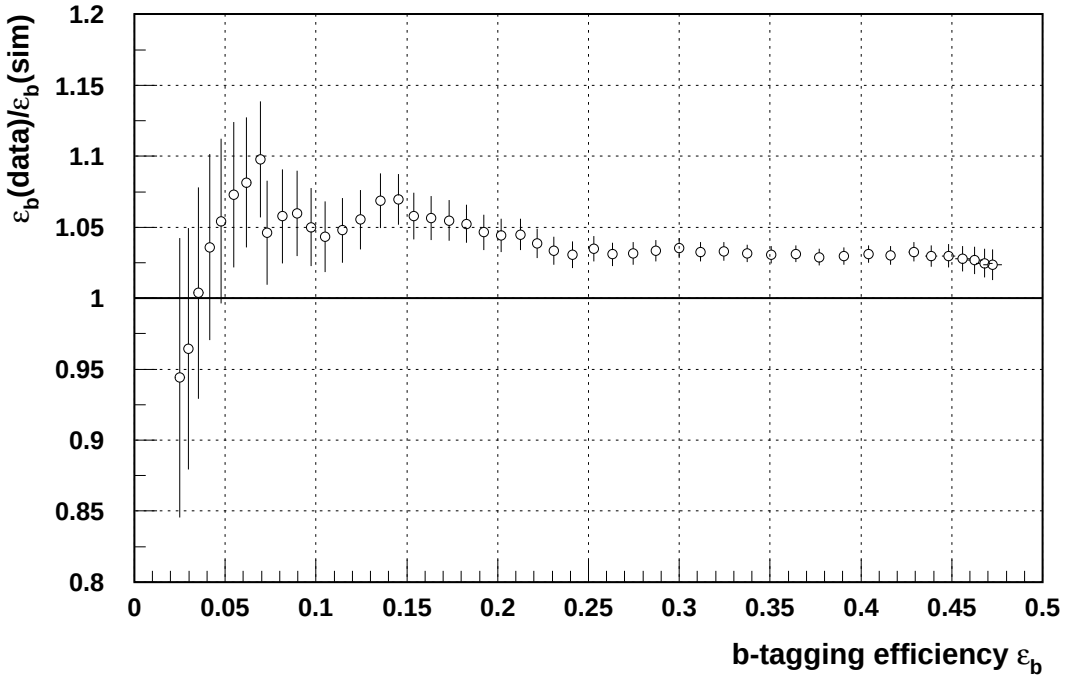

Figure 6: The ratio of the b efficiency ϵ_b measured in 1994 real data and that taken from the simulation as a function of the b efficiency.

The breakdown of the error for the chosen cut on y is given in table 3.

As a cross-check of this measurement, a comparison of R_b as a function of the b efficiency is given in figure 7. The measured value of R_b is stable over a wide range of b purities and therefore of the efficiencies and of the correlation.

5 Energy Dependence

In 1995, data were taken at three different centre of mass energies ($\sqrt{s}$ = 89.44, 91.28, 92.97 GeV). As photon exchange and $\gamma - Z$ interference are strongly suppressed at energies close to the Z resonance, $R_b(\sqrt{s})$ is predicted to be almost constant

Error Source	$\Delta R_b \times 10^3$
Statistical error	± 1.19
Light quark efficiency	± 0.50
Charm efficiency	± 0.50
Correlation	± 0.41
MC statistics	± 0.51
Acceptance bias	± 0.14
Total	± 1.54

Table 3: Sources of errors for the measurement of R_b.

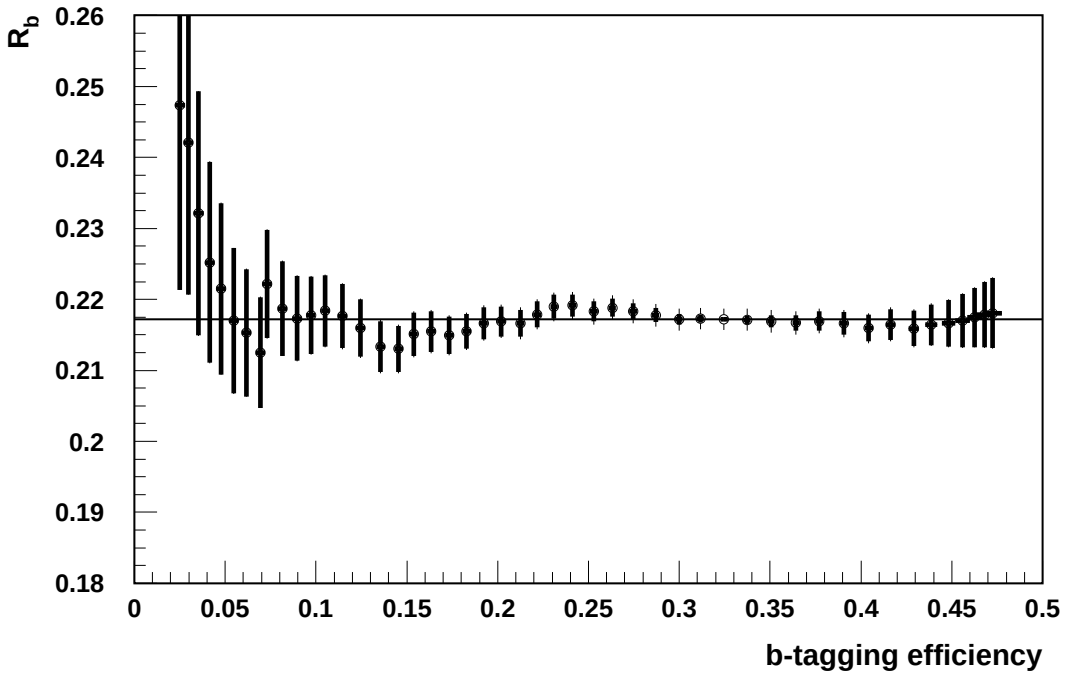

Figure 7: The value of R_b with its total error as a function of the b efficiency for 1994 data. The horizontal line corresponds to the value measured at the reference point, $-\log_{10} y \geq 1$, that corresponds to $\epsilon_b = 32.46\%$.

in the Standard Model. However, if R_b is affected by the interference of the Z with a Z' almost degenerate in mass, as suggested by Caravaglios and Ross [24], some energy dependence can be expected if the mass and width of the Z' are not exactly equal to those of the Z. Since the b-tagging efficiency varies only very little within the energy range considered here, no complicated single to double tag comparison is needed to measure $\frac{R_b(\sqrt{s})}{R_b(91.28\,\mathrm{GeV})}$. Instead, simply the ratio of the fraction of tagged events can be used, with very small corrections due to changes in the b-tagging efficiency and almost negligible corrections due to background. These corrections were calculated using the Monte Carlo simulation. The measurement was performed using event probabilities instead of hemisphere probabilities. Several different values of the event probability cut were used, and a minimum statistical error was found at a b-purity of 79%. At this value of the cut, the b-tagging efficiency varied by a relative amount of $\pm 0.1\%$ with respect to that at the Z peak and was about 81%, while the efficiency to tag c (uds) events was about 21% (2%). The following ratios were found:

$$R_- = \frac{R_b(89.44\,\mathrm{GeV})}{R_b(91.28\,\mathrm{GeV})} = 0.9870 \pm 0.0114,$$
$$R_+ = \frac{R_b(92.97\,\mathrm{GeV})}{R_b(91.28\,\mathrm{GeV})} = 1.0056 \pm 0.0096.$$

The error is statistical only. All systematic uncertainties were found to be negligible. The Standard Model predicts a ratio of 0.997 (0.998) for R_- (R_+). Figure 8 shows the stability of the measurement as a function of the b-purity. Combining with the published values for the 1993 energy scan [3] yields:

$$\frac{R_b(89.46\,\mathrm{GeV})}{R_b(91.27\,\mathrm{GeV})} = 0.9852 \pm 0.0091,$$
$$\frac{R_b(93.00\,\mathrm{GeV})}{R_b(91.27\,\mathrm{GeV})} = 1.0033 \pm 0.0082.$$

Figure 9 compares the result with the Standard Model prediction. The values at higher energies are taken from [25].

6 The Multivariate Analysis

In the impact parameter analysis, hemispheres are tagged simply as b and non-b. This leads to two equations with six unknowns: R_b, ϵ_b, R_c, ϵ_{uds}, ϵ_c and ρ. Three of them, ρ and the efficiencies ϵ_{uds} and ϵ_c, are then taken from simulation and R_c is fixed to the Standard Model value. If the number of equations for physical observables was larger than the number of unknowns, the latter could be extracted directly from the data and the simulation would be required only to estimate systematic errors and the influence of hemisphere correlations. This is the principle of the multivariate approach to measuring R_b.

6.1 The method

With some tagging algorithm, hadronic events containing $N_F = 3$ flavours (uds, c and b) are classified into N_T tagging categories or tags. The set of observables is then the matrix D_{IJ} with I,J = 1,...,N_T, defined as the observed fraction of events tagged as I and J for

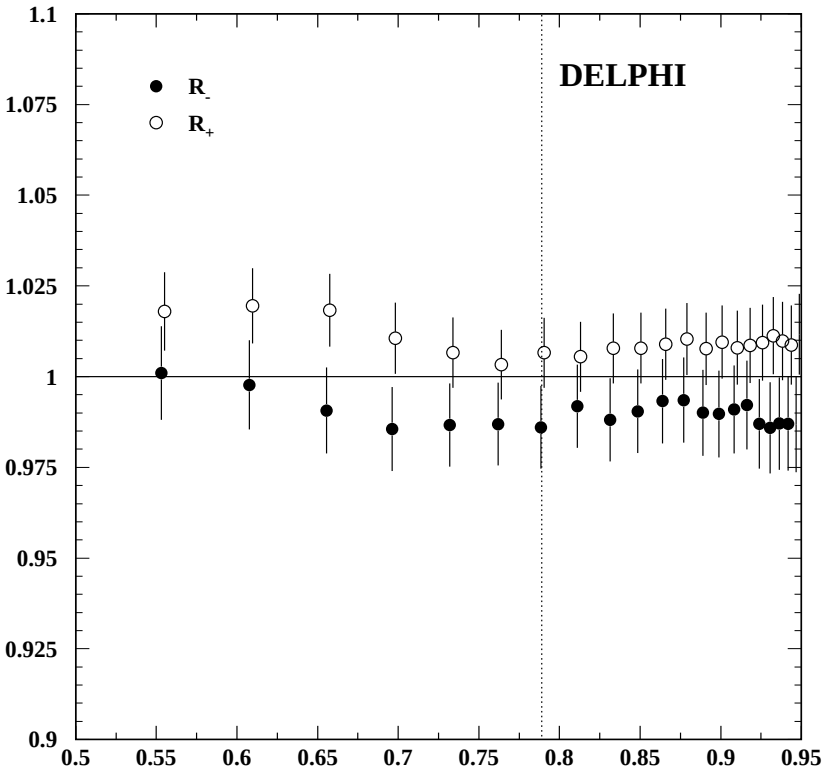

Figure 8: Ratio of the off-peak and on-peak R_b values as a function of the b-purity. The vertical dotted line marks the cut used for the central values.

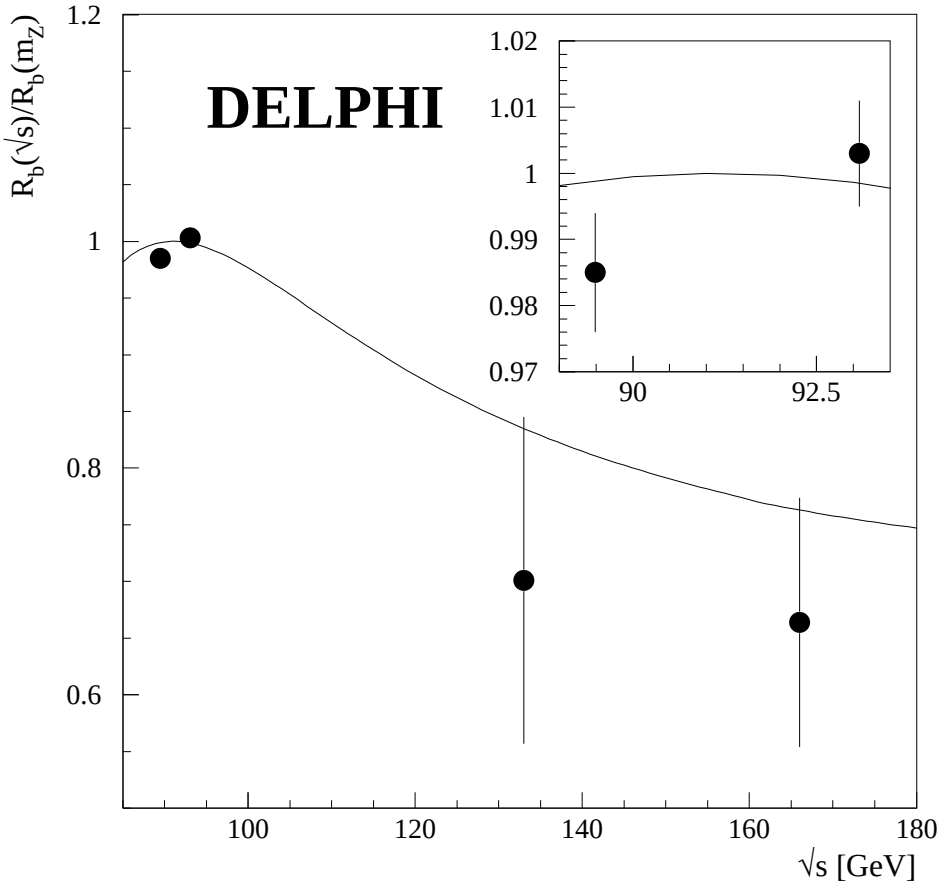

Figure 9: Ratio of the off-peak and on-peak R_b values as a function of $\sqrt{s}$. The solid line shows the Standard Model prediction.

hemispheres 1 and 2 respectively. The corresponding expected fraction of events T_{IJ} can be written as

$$T_{IJ} = \sum_q \epsilon_I^q \epsilon_J^q (1 + \rho_{IJ}^q) R_q. \tag{7}$$

In equation (7), R_q are the flavour fractions, verifying $\sum_q R_q = 1$, and ϵ_I^q is the probability to classify a hemisphere of flavour $q = uds$, c, b in tag I. The matrix ρ_{IJ}^q accounts for hemisphere-hemisphere tagging correlations for flavour q and tags I and J. Assuming that all the hadronic hemispheres are classified in one tag, the conditions

$$\sum_I \epsilon_I^q = 1, \quad q = uds, c, b \tag{8}$$

and

$$\sum_I \epsilon_I^q \epsilon_J^q \rho_{IJ}^q = 0, \quad q = uds, c, b; \quad J = 1, ..., N_T \tag{9}$$

are satisfied. The $N_T(N_T + 1)/2 - 1$ independent measurements are therefore described by the following set of unknown independent parameters: $(N_F - 1)$ flavour fractions, $N_F(N_T - 1)$ efficiencies and $N_F N_T(N_T - 1)/2$ correlation coefficients. As the correlation is small, the independent correction factors ρ_{IJ}^q for $I, J \neq N_T$ can be taken from simulation. Thus the global counting of degrees of freedom requires at least $N_T = 6$. The fit of the D_{IJ} observables to equation (7), verifying (8) and (9), should provide, in principle, the full efficiency matrix ϵ_I^q together with the flavour fractions R_q and the correlation coefficients ρ_{IJ}^q for I or J equal to N_T. The method of Lagrange multipliers is appropriate to solve this problem [19, 20]. However, in practice, it is not possible because of the rotation degeneracy described in [21]. This problem can be avoided if some additional constraints are used. In previous results, DELPHI used a second set of observables [3]. However, this solution has been proven to be statistically limited and new solutions are needed. In the analysis presented here, the problem is resolved by taking from simulation the backgrounds of one of the tags and fixing R_c to its electroweak theory prediction. Systematic dependences of R_b on these three parameters can be reduced if the corresponding tag has a high b purity (b-tight tag). The systematic error will reflect the uncertainties in the simulation calculations of the background efficiencies of the b-tight tag, $\epsilon_{b-tight}^{uds}$ and $\epsilon_{b-tight}^{c}$, and the correlations ρ_{IJ}^q with $I, J \neq N_T$. The result will be given as a function of the assumed value of R_c. Even though the smallest number of tags to measure R_b is now $N_T = 4$, the choice $N_T = 6$ was made in order to overconstrain the problem and to minimize the error. The number of independent observables is therefore 20 with 14 independent unknowns: 13 efficiencies and R_b.

6.2 The hemisphere multitag definition

To provide the six hemisphere tags, the combined lifetime tag used in the impact parameter analysis and defined by equation (2) is complemented with two additional flavour tagging algorithms. The tags are constructed in an attempt to isolate uds, c and b quarks with high efficiency and purity, using exclusively the information provided by each hemisphere. In particular, the primary vertex is reconstructed in all the tagging methods independently in the two hemispheres, so the hemisphere correlations are kept small.

The *multivariate flavour tagging* algorithm [22] is based on the large mass and relatively long lifetime of the b quark and some event shape properties of its decays. All the available information is combined using multivariate techniques. The lifetime information exploits the large impact parameters of tracks coming from B decays together with a search for secondary vertices and their invariant masses. Finally, the lifetime information is combined with event shape properties of the B decays like large transverse momentum of the tracks with respect to the jet axis, rapidity distributions and the boosted sphericity. A total of $N = 13$ variables is finally adopted. See reference [22] for a detailed description of the variables.

The probabilities p_q^λ of observing a value of the variable λ for a hemisphere of flavour q are computed using model distributions taken from simulation. An estimate of the probability to observe simultaneously a set of N variables is given by

$$\mathcal{P}_q = \frac{n_q \prod_{\lambda=1}^{N} p_q^\lambda}{\sum_{q'} n_{q'} \prod_{\lambda=1}^{N} p_{q'}^\lambda}, \tag{10}$$

where $n_q = 1$ for $q = c, b$ and $n_q = 3$ for $q = uds$ hemispheres. The empirical factor 3 assigned to uds reflects the fact that this flavour is the sum of the three lighter flavours u, d and s, which are taken together because their distributions are similar. With this formulation the 5 flavours have the same weight.

In practice, what counts in comparing flavours are ratios of probabilities or differences of their logarithms. For this reason new estimators $\mathcal{L}_q$, called flavour likelihoods, are introduced. $\mathcal{L}_b$ is defined as

$$\mathcal{L}_b = \frac{2 \ln \mathcal{P}_b - \ln \mathcal{P}_{uds} - \ln \mathcal{P}_c}{3} \tag{11}$$

and similarly for $\mathcal{L}_{uds}$ and $\mathcal{L}_c$. A hemisphere can be classified according to the largest flavour likelihood (which is positive). Based on the best likelihood, each primary tag can be subdivided into subtags according to a set of given cuts.

Similarly to the multivariate approach, the *flavour confidences* method [23] is based not only on the track impact parameters but also on two other kinematic variables, the track momentum and the angle with respect to the jet axis. The track information is used differently in both techniques, so the overlap between them is expected not to be complete and interesting gains in performances can be obtained in a combination. The method uses the simulation to build a function $\mathcal{C}_q$ which gives the fraction of tracks which come from uds, c and b quarks in a bin of three particle characteristics: impact parameter over its error, momentum and angle to the jet axis. There are kinematic effects in the decay of B hadrons which produce correlations between the three quantities, but they are automatically taken into account by the three-dimensional binning. The individual flavour confidences are finally combined to make the hemisphere tag:

$$\mathcal{CONF}_q = \frac{n_q \prod_i \mathcal{C}_q^i}{\sum_{q'} n_{q'} \prod_i \mathcal{C}_{q'}^i}, \tag{12}$$

$\mathcal{C}_q^i$ being the q flavour confidence for track i.

The two tags, multivariate and confidences, can be combined using a simple linear combination for each flavour. In order to be homogeneous with the multivariate flavour likelihood $\mathcal{L}_q$, we have to take the logarithm of the difference from unity of each flavour confidence:

$$\Delta_q = (1-\alpha)\mathcal{L}_q - \alpha \ln(1 - \mathcal{CONF}_q) \tag{13}$$

The quantities Δ_q are called flavour multivariate discriminators and will be finally the basis of the classification. This way to combine has been proven to be the best of several tried. It could also be possible to optimize a different value of α for each flavour, but it happens that the same value optimize the three flavours. The quoted value was $\alpha = 0.8$. The apparently high ratio $\alpha/(1-\alpha) = 4$ is due to the fact that the range definition of the multivariate flavour likelihood is higher than that of the flavour confidences. It corresponds approximately to an equal weight of the two components. Figure 10 shows the distributions of the flavour multivariate discriminators for data and simulation. It can be seen that the agreement between data and Monte Carlo is reasonable. In any case, the analysis is insensitive to small disagreements as they affect only the efficiencies, which are fitted from data. The effects on the correlation are discussed in section 6.4.

The definition of the tags in terms of the three available tagging techniques is given in table 4. Three of the six tags are designed to identify b quarks, one c quarks and one uds quarks. The remaining tag (no-tag) contains all hadronic hemispheres not contained in one of the previous tags, in order to verify experimentally the condition (8). To avoid double counting, a priority is assigned to each tag and if a hemisphere satisfies more than one tag, it is assigned to the tag with the highest priority.

Tag	Condition	Priority
b-tight	$y \leq y_0$	1
b-standard	$\Delta_b > \Delta_{b,0}^{up}$	2
b-loose	$\Delta_b > \Delta_{b,0}^{low}$	3
charm	$\Delta_c > \Delta_{c,0}$	4
uds	$\Delta_{uds} > \Delta_{uds,0}$	5
no-tag		6

Table 4: Definition of the hemisphere tags.

The b-tight tag has the highest impact on R_b and the cut $-\log_{10} y_0$ is fixed at 1.2 to minimize the total error. All other cuts are chosen in order to obtain good efficiencies with reasonable backgrounds in the affected tags. They were taken to be $\Delta_{b,0}^{up}$=3.5, $\Delta_{b,0}^{low}$=1.2, $\Delta_{c,0}$=0.65 and $\Delta_{uds,0}$=3.2. The Monte Carlo expectations for the efficiencies are given separately for 1994 and 1995 in table 5. This table is a measure of the performance of the tags and tagging techniques all working simultaneously. In this analysis of R_b, only the charm and light quark backgrounds of the b-tight tag are taken from simulation. Therefore the light and charm quark systematic errors of the impact parameter analysis are valid for this measurement of R_b, but computed at a harder cut. All the other efficiencies are measured directly from the data and can be used as a powerful cross-check of the analysis.

Compared with the impact parameter analysis in which only b-tight tagged hemispheres are used (single tag), in this multitag analysis all hadronic hemispheres are tagged, allowing the statistical accuracy to be increased. The systematic uncertainty on R_b is also improved.

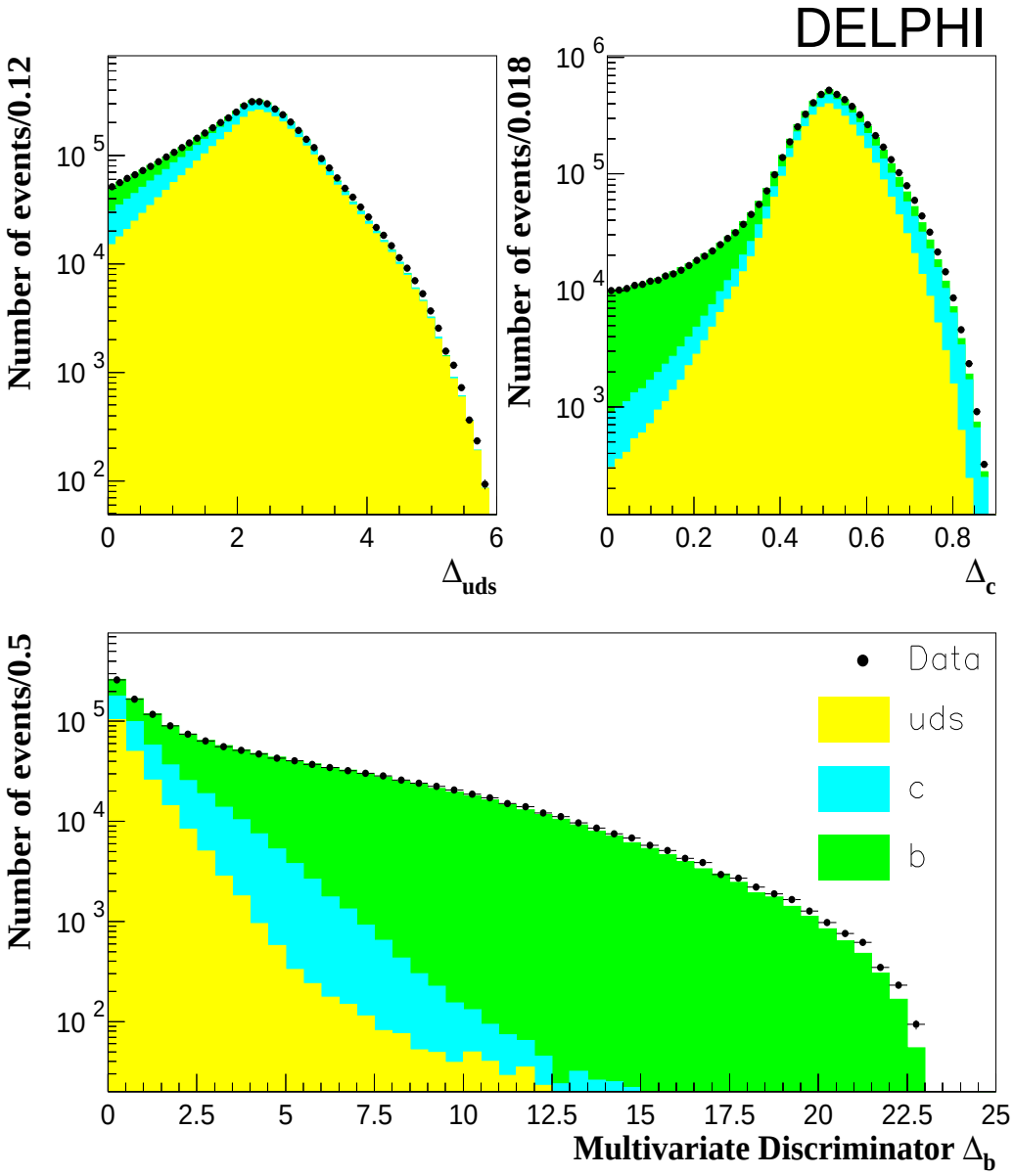

Figure 10: Distribution of the multivariate discriminator Δ_q in the *uds*, *c* and *b* tags for data and simulation. The different types of shading show the different flavour contributions to the simulated event sample. The simulation distributions are normalized to the data statistics. Only the positive region of Δ_q is shown.

Tag	1994 ϵ^{uds}	1994 ϵ^{c}	1994 ϵ^{b}	1995 ϵ^{uds}	1995 ϵ^{c}	1995 ϵ^{b}
b-tight	0.00052	0.00407	0.28404	0.00040	0.00376	0.27453
b-standard	0.00131	0.02782	0.15751	0.00120	0.02678	0.15558
b-loose	0.01200	0.07877	0.15108	0.01212	0.07812	0.15380
charm	0.05174	0.16143	0.05171	0.05415	0.16128	0.05295
uds	0.12054	0.03123	0.00488	0.11678	0.03083	0.00479
no-tag	0.81390	0.69667	0.35078	0.81525	0.69923	0.35835

Table 5: Monte Carlo results for the tagging efficiencies at the nominal cuts.

6.3 The measurement of R_b

In this analysis, the criteria used to select tracks and to identify hadronic Z decays are basically the same as described in section 3, with the main difference that 5 reconstructed charged particles were required. 1370354 (664676) hadronic Z decays were selected in 1994 (1995), of which 828168 (400482) passed the $|\cos\theta_{thrust}| < 0.65$ cut. The bias towards b events in the selected sample was found to be small, $(0.69 \pm 0.13) \times 10^{-3}$ in 1994 and $(1.18 \pm 0.26) \times 10^{-3}$ in 1995, and was corrected for. The uncertainty due to the event selection is dominated by statistics.

The experimentally measured numbers of doubly tagged events which passed the $|\cos\theta_{thrust}|$ cut are given in table 6 for 1994 and 1995 separately. The fit of R_b and the efficiencies to these numbers gives the results

$$R_b = 0.21617 \pm 0.00100(stat.)$$

with $\chi^2/ndof = 4.76/6$ for 1994 and

$$R_b = 0.21688 \pm 0.00144(stat.)$$

with $\chi^2/ndof = 4.32/6$ for 1995. The errors are only statistical. These results have also been corrected for tau background. The efficiencies obtained from the same fits within statistical errors are shown in table 7. They can be compared with the simulation predictions of table 5. For a complete comparison, an estimate of the systematic errors must be included.

6.4 Systematic errors

The systematic errors are due to the quantities estimated from simulation: event selection bias, light and charm quark backgrounds in the b-tight tag and hemisphere correlations.

6.4.1 Light and charm quark efficiency uncertainties

The sensitivity of R_b to light and charm quark uncertainties is the same as in the single tag method used in the impact parameter analysis. However, the corresponding uncertainties are smaller because of the harder cut on $\log_{10} y$ defining the b-tight tag, which reduces the background uds and c efficiencies by factors of about 1.2 and 1.5 respectively. They have been estimated by following exactly the procedure described in section 4.3. Table 8

	1994					
Tag	b-tight	b-standard	b-loose	charm	uds	no-tag
b-tight	15809					
b-standard	17048	4656				
b-loose	16006	9091	5050			
charm	5918	4396	7619	7218		
uds	667	778	2619	10436	9474	
no-tag	36111	25453	43026	91054	110430	405309
	1995					
Tag	b-tight	b-standard	b-loose	charm	uds	no-tag
b-tight	7804					
b-standard	7752	1965				
b-loose	7695	4266	2394			
charm	3005	2088	3832	3860		
uds	290	331	1262	5321	4241	
no-tag	17937	11785	20680	46621	51309	196044

Table 6: Measured numbers of doubly tagged events, passing the $|\cos\theta_{thrust}|$ cut.

shows the breakdown of these uncertainties in the different sources. The charm physics sources of systematics are detailed in table 1.

6.4.2 Hemisphere correlation uncertainties

The ρ^q_{IJ} hemisphere correlation corrections as estimated from simulation together with their sensitivities are given in the second column of table 9, where the errors are due to simulation statistics. Only the relevant correlations with a sensitivity higher than 0.010 are shown. The sensitivity is defined as the relative change on R_b due to a change of a given correlation, $\frac{\Delta R_b}{R_b \Delta \rho^q_{IJ}}$. The sensitivity of this measurement of R_b to $\rho^b_{b-tight,b-tight}$ is 0.805, compared to unity in the impact parameter analysis. However, as shown in the table, there are other correlations with important sensitivities which have zero sensitivity in the impact parameter analysis. As explained in section 6.1, correlations containing the no-tag category (I or $J = N_T$) were determined from the fit to data, so they have a negligible sensitivity on the analysis.

Systematic errors on ρ^q_{IJ} arise from uncertainties in the simulation both of uds, c and b physics and of the vertex detector acceptance and gluon radiation.

Effects from $udscb$ physics

Uncertainties in physical parameters used in the simulation of correlations are calculated by varying these physics inputs within their experimental ranges around their central values, according to the prescription given in reference [17]. For each variation of these physical parameters, obtained by reweighting the simulation, all the correlation correction factors are recomputed, allowing a new determination of R_b. The change observed on R_b is assigned as systematic error. Table 10 summarizes the errors on R_b due to these physical uncertainties.

Tag	1994 ϵ^{uds}	ϵ^{c}	ϵ^{b}
b-tight	0.00052	0.00407	0.2950 ± 0.0012
b-standard	0.0016 ± 0.0002	0.0262 ± 0.0015	0.1593 ± 0.0007
b-loose	0.0119 ± 0.0004	0.0799 ± 0.0020	0.1498 ± 0.0008
charm	0.0638 ± 0.0005	0.1754 ± 0.0016	0.0536 ± 0.0006
uds	0.1308 ± 0.0005	0.0331 ± 0.0016	0.0052 ± 0.0002
no-tag	0.7914 ± 0.0008	0.6814 ± 0.0035	0.3371 ± 0.0013
Tag	1995 ϵ^{uds}	ϵ^{c}	ϵ^{b}
b-tight	0.00049	0.00376	0.2962 ± 0.0017
b-standard	0.0016 ± 0.0002	0.0244 ± 0.0024	0.1492 ± 0.0010
b-loose	0.0130 ± 0.0006	0.0735 ± 0.0029	0.1498 ± 0.0012
charm	0.0690 ± 0.0008	0.1825 ± 0.0024	0.0560 ± 0.0009
uds	0.1254 ± 0.0007	0.0350 ± 0.0024	0.0044 ± 0.0003
no-tag	0.7906 ± 0.0012	0.6808 ± 0.0052	0.3444 ± 0.0019

Table 7: Tagging efficiencies with statistical errors for data as measured from the fit at the nominal cuts. For a complete comparison of the fit results with the simulation an estimate of the systematic error must be included.

Source	$\Delta\epsilon_I^{uds}/\epsilon_I^{uds}$	$\Delta\epsilon_I^{c}/\epsilon_I^{c}$	$\Delta R_b \times 10^4$
Tracking	0.054	0.022	$\pm 1.57/1.40$
K^0, Λ^0, photons, etc.	0.014	-	$\mp 0.26/0.28$
$g \to c\bar{c}: \ (2.38 \pm 0.48)\%$ per event	0.159	0.024	$\mp 3.63/3.36$
$g \to b\bar{b}/g \to c\bar{c}: \ 0.13 \pm 0.04$	0.144	0.021	$\mp 3.27/3.05$
Charm physics	-	0.066	$\mp 3.13/2.75$
Total $udsc$ background systematics	0.222	0.076	$\pm 6.02/5.50$
MC statistics (1994/1995)	0.025/0.055	0.017/0.037	$\pm 0.96/1.90$

Table 8: Light and charm quark systematics on R_b at cut $-\log_{10} y \geq 1.2$ for the 1994/1995 data.

Angular effects and gluon radiation

Remaining errors on the correlations not due to physics simulation can be estimated by isolating the contributions to correlations and comparing their effect in data and simulation. The variables used to isolate the correlation sources are exactly the same as described in the impact parameter analysis: the polar and azimuthal angles and p_{jet}.

The contribution to ρ_{IJ}^{q} from one of the above variables Θ can be determined through the following expression:

$$\rho_{IJ}^{q,\Theta} = \frac{\sum_\Theta f_q(\Theta)\left[\epsilon^q_{I,same}(\Theta)\epsilon^q_{J,oppo}(\Theta) \ + \ \epsilon^q_{J,same}(\Theta)\epsilon^q_{I,oppo}(\Theta)\right]}{2\left[\sum_\Theta f_q(\Theta)\epsilon^q_{I,same}(\Theta)\right]\ \left[\sum_\Theta f_q(\Theta)\epsilon^q_{J,same}(\Theta)\right]} - 1, \qquad (14)$$

where $f_q(\Theta)$ is the fraction of q hemispheres as a function of the variable Θ and $\epsilon^q_{I,same}(\Theta)$ and $\epsilon^q_{I,oppo}(\Theta)$ are the efficiencies to tag a hemisphere of flavour q as a function of Θ in the same and opposite hemisphere respectively.

	MC global correction	Sensitivity	$\cos\theta_{thurst}$		ϕ_{thurst}		p_{jet}	
			MC correction	Data correction	MC correction	Data correction	MC correction	Data correction
b correlations								
$\rho^b_{b-tight,b-tight}$	0.0187 ± 0.0027	0.805	0.0057	0.0056	0.0006	0.0011	0.0115	0.0130
$\rho^b_{b-tight,b-standard}$	0.0036 ± 0.0027	0.236	0.0031	0.0032	0.0006	0.0009	0.0100	0.0100
$\rho^b_{b-tight,b-loose}$	-0.0020 ± 0.0028	0.140	0.0012	0.0016	-0.0007	0.0010	0.0042	0.0051
$\rho^b_{b-tight,charm}$	0.0104 ± 0.0053	-0.040	-0.0008	-0.0011	0.0028	0.0010	0.0055	0.0066
$\rho^b_{b-standard,b-standard}$	0.0047 ± 0.0050	-0.082	0.0044	0.0037	0.0007	0.0001	0.0083	0.0071
$\rho^b_{b-standard,b-loose}$	-0.0003 ± 0.0042	-0.072	0.0037	0.0029	0.0008	0.0005	0.0035	0.0037
$\rho^b_{b-standard,charm}$	-0.0094 ± 0.0077	0.028	-0.0090	-0.0015	0.0004	0.0037	0.0047	0.0045
$\rho^b_{b-loose,b-loose}$	0.0144 ± 0.0052	-0.037	0.0036	0.0024	0.0013	0.0010	0.0022	0.0025
$\rho^b_{b-loose,charm}$	-0.0139 ± 0.0079	0.019	-0.0101	-0.0038	-0.0001	0.0001	0.0029	0.0035
c correlations								
$\rho^c_{b-standard,charm}$	-0.0469 ± 0.0197	0.012	-0.0032	-0.0024	0.0018	0.0007	0.0124	0.0083
$\rho^c_{b-loose,charm}$	-0.0015 ± 0.0115	0.025	-0.0070	-0.0055	0.0009	-0.0024	0.0142	0.0193
$\rho^c_{charm,charm}$	0.0350 ± 0.0093	-0.015	0.0178	0.0110	0.0022	0.0005	0.0116	0.0148
uds correlations								
$\rho^{uds}_{charm,uds}$	0.0219 ± 0.0091	0.020	0.0104	0.0104	0.0008	0.0001	0.0184	0.0172
$\rho^{uds}_{uds,uds}$	0.0778 ± 0.0067	0.022	0.0119	0.0108	0.0040	0.0018	0.0374	0.0276

Table 9: b, c and uds correlations with major sensitivity (> 0.010) on R_b at the nominal cuts for the 1994 data. For the 1995 data the correlations obtained are similar.

Source	$\Delta R_b \times 10^4$
Two b quarks in same hemisphere: $\pm 30\%$	∓ 0.84
$g \to c\bar{c}$: $(2.38 \pm 0.48)\%$ per event	∓ 0.05
$g \to b\bar{b}/g \to c\bar{c}$: 0.13 ± 0.04	∓ 0.05
b fragmentation $\langle x_E(b) \rangle$: 0.702 ± 0.008	∓ 0.53
B decay multiplicity: 5.25 ± 0.35	∓ 2.01
B_s fraction: 0.112 ± 0.019	∓ 0.56
Λ_b fraction: 0.132 ± 0.041	∓ 0.55
Average B lifetime: 1.55 ± 0.04 ps	∓ 0.02
Charm physics	∓ 0.32
Total uds, c and b physics correlation error	∓ 2.40
Angular effects (1994/1995)	$\pm 3.55/2.92$
Gluon radiation (1994/1995)	$\pm 2.46/1.96$
MC statistics (1994/1995)	$\pm 5.52/9.23$

Table 10: Systematic errors due to hemisphere correlations for the multivariate analysis.

The contribution $\rho_{IJ}^{q,\Theta}$ can easily be computed for Monte Carlo where the flavour q is known. However, comparison of data and Monte Carlo requires the experimental isolation of this flavour in the data. This flavour isolation was obtained successfully for uds and b quarks using a soft multivariate tag. No c quark selection was obtained with success due to the small c event statistics and the rather poor c quark purification. However this was proven not to be a problem because of the small sensitivity of R_b to c correlations. The uds and b selections were done imposing the cuts $\Delta_{uds} > 1.5$ and $\Delta_b > -0.5$ respectively on the opposite hemisphere to the tested one. The resulting hemisphere b efficiencies were 11.7%, 35.5% and 79.2% for uds, c and b flavours respectively. The hemisphere uds efficiencies were 82.4%, 52.3% and 15.0% for uds, c and b flavours respectively. The result was then scaled by the ratio of the correlations in pure q events and in the selected uds and b events obtained from simulation; c correlations were obtained by scaling using all events. Table 9 shows the results of this procedure for each of the testing variables, for data and simulation. It can be seen that these three variables account for most of the global correlation correction and other correlation sources have a negligible effect on the correlation systematics.

The error assignment was performed on the basis of the R_b difference when correlations from data and simulation were taken. The errors for the three sources were added quadratically and the quoted uncertainties are listed in table 10. It must be stressed that this systematic error can not be attributed only to differences between data and Monte Carlo for the particular flavour, but they can also be due to imperfections of the flavour isolation and scaling.

6.5 Results and consistency checks

In summary, the final result with the 1994 data is

$$R_b = 0.21617 \pm 0.00100(stat.) \pm 0.00096(syst.) - 0.024 \times (R_c - 0.172)$$

and for the 1995 data is

$$R_b = 0.21688 \pm 0.00144(stat.) \pm 0.00120(syst.) - 0.024 \times (R_c - 0.172),$$

where the first error is statistical and the second systematic. The explicit dependence of this measurement with the assumed R_c value is also given.

The results are compatible and can be combined, with the following assumptions:

- all statistical errors are assumed to be independent;
- the errors in the hemisphere correlations due to gluon radiation are assumed to be fully correlated, but those from angular effects are taken uncorrelated;
- the errors due to uds, c and b physics simulation inputs are assumed to be fully correlated, as well as the errors due to detector effects on the estimate of light and charm quark efficiencies.

With these assumptions, the result for the combined 1994/1995 data is:

$$R_b = 0.21640 \pm 0.00082(stat.) \pm 0.00088(syst.) - 0.024 \times (R_c - 0.172).$$

The b hemisphere tagging efficiency was found to be $\epsilon^b_{b-tight} = 0.2950 \pm 0.0012$ (0.2962 ± 0.0017), compared to the simulation estimate of 0.284 (0.275), for 1994 (1995) data. As previously, the real data are about 4% (7%) more efficient than simulation. The purity at the working point for this measurement is 98.4%.

Figure 11 shows the stability of the final R_b result as a function of the cut on $\log_{10} y$ defining the b-tight tag, together with the change of the contributions to the total error. It can be seen that the best error is obtained at cut $-\log_{10} y \geq 1.2$. The cut at 0.0 corresponds to an efficiency/purity of 44.0%/91.6%, compared to 21.0%/99.4% at cut 2.0. Figure 12 shows the stability of R_b as a function of all other cuts $\Delta^{up}_{b,0}$, $\Delta^{low}_{b,0}$, $\Delta_{c,0}$ and $\Delta_{uds,0}$ defining the hemisphere tags. Table 11 reports the full breakdown of the error on this measurement.

This measurement is highly correlated with that obtained with the impact parameter analysis and both are consistent. In order to check this easily, the measurement of R_b was performed at cut $-\log_{10} y \geq 1.0$ using the multitag and single tag methods. The multitag approach provided the results $R_b = 0.21615 \pm 0.00095(stat.)$ for the 1994 data. To check that the slightly different event selection does not shift the results, R_b was again measured using the single tag approach used in the impact parameter analysis. The values $R_b = 0.21685 \pm 0.00113(stat.)$ was obtained for 1994, in agreement (within statistical errors) with the result quoted in section 4.

The difference between these R_b results is not only due to their statistical differences. The sensitivity of both approaches to light and charm quark efficiency uncertainties is the same, and therefore the systematic errors due to uds and c backgrounds are fully correlated. However, the sensitivities to correlations are different. In fact, the sensitivity of the multitag measurement to $\rho^b_{b-tight,b-tight}$ at cut $-\log_{10} y \geq 1.0$ is 0.805, compared to the sensitivity of unity of the single tag analysis. In this way, the correlation error as obtained in the impact parameter analysis, $\Delta\rho^b_{b-tight,b-tight} = \pm 0.0030$ in 1994 induces an error on R_b of 0.00064 and 0.00055 for the single tag and multitag methods respectively. Therefore, the part of the error due to correlations which is uncorrelated between the multitag and the single tag analyses is 0.00033. Combining this error with the statistical

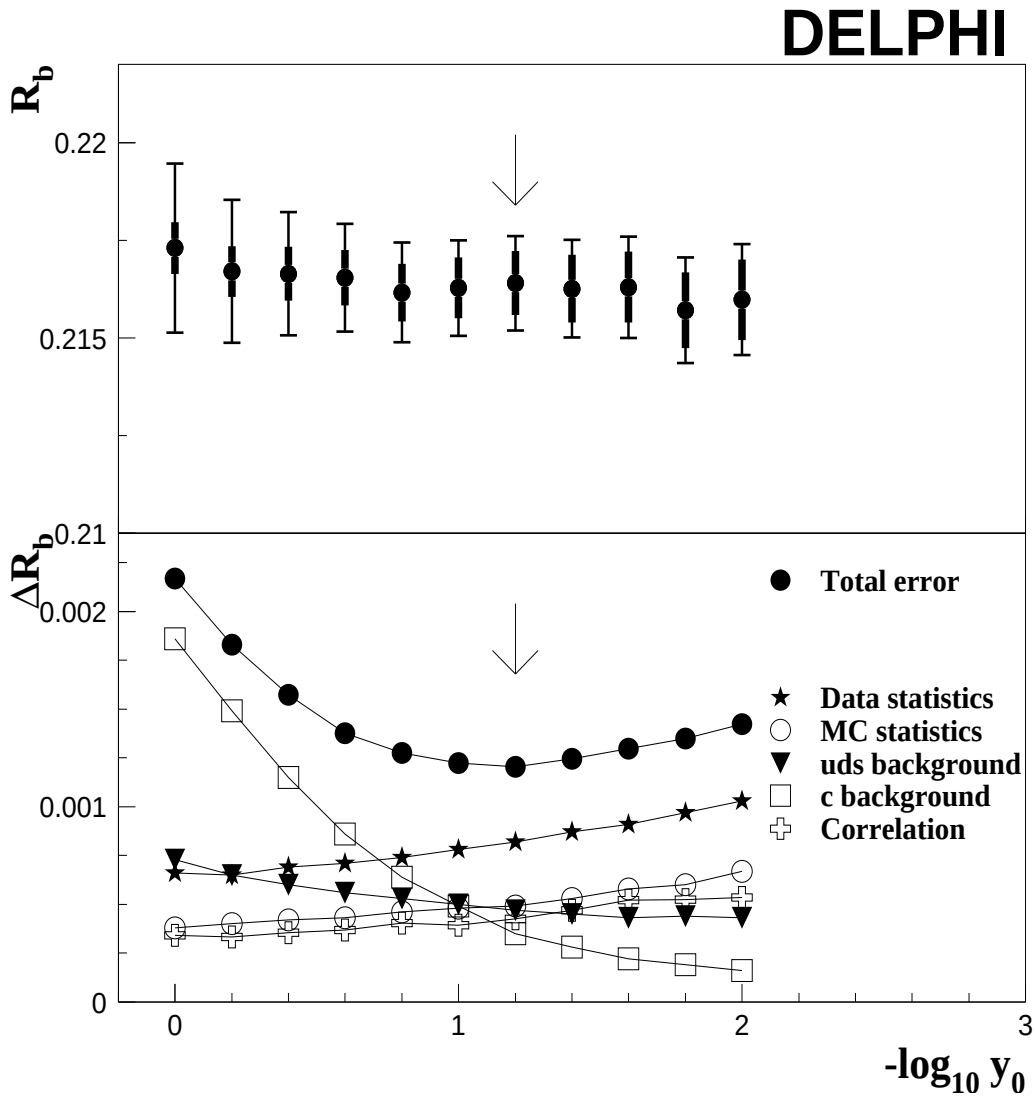

Figure 11: Stability of the R_b result as a function of the cut $\log_{10} y_0$ defining the b-tight tag, together with the change of the contributions to the total error. The best error is obtained at cut 1.2. In the upper plot the thick error bar represents the statistical uncertainty and the narrow one is the total error.

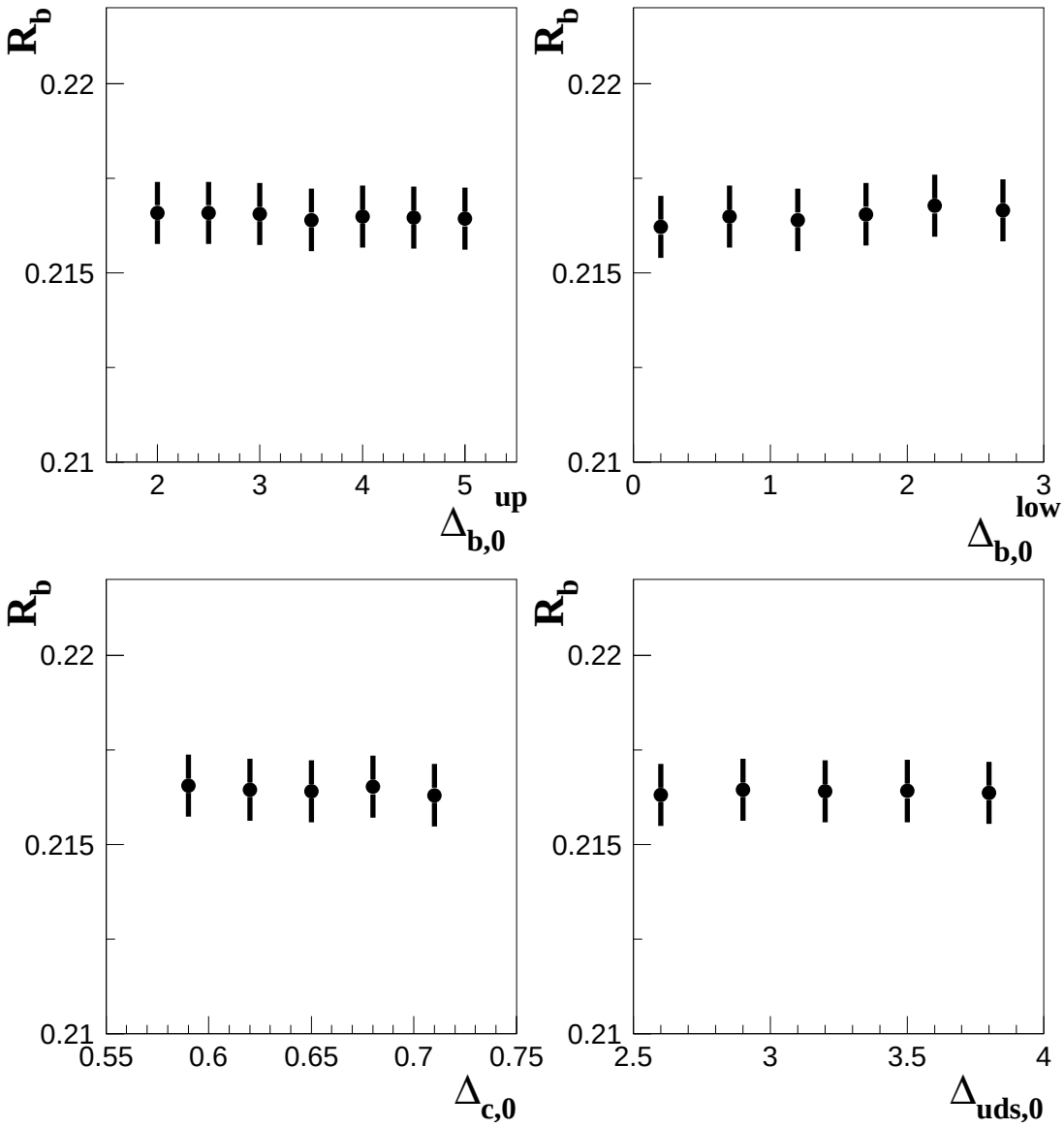

Figure 12: Stability of the R_b result as a function of the cuts $\Delta_{b,0}^{up}$, $\Delta_{b,0}^{low}$, $\Delta_{c,0}$ and $\Delta_{uds,0}$ defining the b-standard, b-loose, charm and uds hemisphere tags. Only the statistical errors are shown.

Source	$\Delta R_b \times 10^4$
Data statistics	± 0.00082
MC statistics	± 0.00049
Event selection	± 0.00012
Tracking	± 0.00015
K^0, Λ^0, photons, etc.	∓ 0.00003
$g \to c\bar{c}$: $(2.38 \pm 0.48)\%$ per event	∓ 0.00035
$g \to b\bar{b}/g \to c\bar{c}$: 0.13 ± 0.04	∓ 0.00032
Charm physics	∓ 0.00030
Two b quarks in same hemisphere: $\pm 30\%$	∓ 0.00008
b fragmentation $\langle x_E(b) \rangle$: 0.702 ± 0.008	∓ 0.00006
B decay multiplicity: 5.25 ± 0.35	∓ 0.00020
B_s fraction: 0.112 ± 0.019	∓ 0.00006
Λ_b fraction: 0.132 ± 0.041	∓ 0.00006
Average B lifetime: 1.55 ± 0.04 ps	∓ 0.00000
Angular effects	± 0.00026
Gluon radiation	± 0.00023
Total error	± 0.00120

Table 11: Breakdown of the error on R_b at the nominal cuts for the multivariate analysis.

difference, we obtain a difference between the multitag and single tag measurements of -0.00070 ± 0.00070 and therefore they are well compatible.

In addition, it was checked that the error on $\rho^b_{b-tight,b-tight}$ found with the procedure followed in the impact parameter analysis agreed well with that obtained in this analysis. Flavour isolation and error assignment were done in slightly different ways.

7 Secondary Vertex Analysis

An independent analysis was carried out on data collected in 1994 only, using purely vertex information for the tagging of b quarks. The event selection was similar to that described in section 3, with the exception that at least 7 charged tracks were required to define a hadronic event rather than 6. After the same acceptance cut of $|\cos\theta_{thrust} < 0.65|$, a bias towards b events of (0.0038 ± 0.0002) was found from the simulation and 810000 events were selected from the data for the analysis.

7.1 Secondary vertex search

The search for secondary vertices was made independently inside event hemispheres defined by the plane perpendicular to the event thrust axis. Hemisphere tracks used in the analysis were required to pass the following set of quality cuts:

- $R\phi$ hits in at least 2 layers of the VD,
- an impact parameter in the $R\phi$ plane with respect to the beamspot of less than 0.15 cm,
- a momentum greater than 750 MeV/c.

In addition, an attempt was made to reconstruct and then reject tracks coming from decays of K^0_S and Λ particles and from photon conversions [9]. Candidate secondary vertices were identified by:

- finding first the positions in the $R\phi$ plane of all three-track vertices. Candidates were rejected if any of the following conditions were met: 1) the decay length (L) to the event beam spot was $< \sigma_L$; 2) $L > 3.0\,\mathrm{cm}$; 3) χ^2-probability, $P(\chi^2) < 1\%$.

- Next an attempt was made to add to candidate vertices any track likely to have originated from the same point in space. Each track falling within a cone of half-angle 0.4 radians placed around the candidate vertex momentum vector was fitted in turn to the vertex. That track which contributed the most significant increase in decay length was added permanently to the vertex definition provided that 1) $L > 3\sigma_L$; 2) $L > 3.0\,\mathrm{cm}$; 3) $P(\chi^2) > 1\%$. This procedure was continued until none of the above requirements was met.

- Further tracks were added to the vertex definition if they were deemed to be consistent with the candidate vertex while at the same time inconsistent, within the errors, with the beamspot.

- The last step involved finding a primary (hemisphere) vertex by essentially the same procedure as outlined above for secondary candidates. A *unique* track was defined to be one that was part of a secondary vertex but was not consistent with being part of the primary vertex. Secondary vertex candidates that did not contain a unique track were removed.

Close attention was paid to reducing light quark backgrounds which are potentially poorly modelled in the simulation. For the case of vertices containing two unique tracks that included z-hits, these two tracks were identified and separately fitted to a three-dimensional vertex point. Requiring $P(\chi^2) > 0.1\%$ was found to be an effective cut in removing cases where badly reconstructed tracks might form a vertex in two dimensions but were clearly unassociated with each other once the z-coordinate was considered. To reduce background contamination further, all vertices with only one unique track or a decay length significance less than 4 were rejected.

If after the secondary vertex finding procedure there was more than one candidate vertex in a hemisphere, that vertex with the largest L/σ_L value was chosen to tag the hemisphere.

7.2 Tagging $Z \to b\bar{b}$ events

In order to tag $Z \to b\bar{b}$ events, the output of a neural network [27] was used, with five input variables based only on the properties of the secondary vertices found. They were 1) decay length significance L/σ_L; 2) the number of unique tracks in the secondary vertex; 3) the number of tracks in the primary vertex that were not also associated to a secondary; 4) the number of tracks in common to both the secondary and primary vertices and 5) the vertex rapidity. The variables were carefully chosen for both their flavour discriminating power and their low cross-correlation.

The vertex rapidity was defined as:

$$R = \ln \frac{E + \sqrt{P^2 - {P_t}^2}}{\sqrt{m^2 + {P_t}^2}}, \tag{15}$$

where E, P and P_t are the energy, total momentum and sum transverse momentum of unique tracks in the secondary vertex.

Distributions of all input variables together with the neural network output are shown in figure 13.

The impact parameter tuning used in previous DELPHI analyses [3] and described in [13] was also applied here. The excellent agreement between data and simulation for all variables used in the analysis can be seen in figure 13.

The calculation of R_b followed the double hemisphere method described in section 4.

7.3 Quantities from the simulation

Both the light and charm quark efficiencies were extracted from the simulation with reweighting to reach the input values of various modelling parameters recommended in [17] and listed in table 12. This took account of the rate of gluon splitting to heavy quarks in light quark events, and in the charm sector of differences between the parameters used in the simulation and experimentally measured values of the charmed hadron lifetimes, production fractions and decay modes and charm fragmentation. Further reweighting was carried out to estimate the errors on these efficiencies. There was also a small error due to limited simulation statistics and an error due to details of the modelling of DELPHI detector tracking in the simulation. This error due to detector effects was estimated in a similar way to that described in section 4.3. It should be noted that the simulation sample used to train the neural network, which amounted to 16% of the total, was excluded from the determination of background efficiencies.

Due to the interplay between statistical and systematic errors, the total error on the measurement of R_b reached a minimum at a cut on the neural network output of 0.86, as shown in figure 14. In the simulation, the b purity at this cut was 95.1% and the b-tagging efficiency was 26.3%. All numbers quoted below and the final result correspond to a cut of 0.86.

The light and charm quark efficiencies extracted from the simulation were:

$$\epsilon_l = (0.093 \pm 0.015) \times 10^{-2}; \tag{16}$$

$$\epsilon_c = (1.28 \pm 0.08) \times 10^{-2}. \tag{17}$$

These are the total errors on the efficiencies and their contributions to the systematic error on R_b are broken down in table 12. The efficiencies for tagging each quark flavour in the simulation are shown across a range of b purities in figure 15. The good agreement between the b-tagging efficiencies observed in the simulation and those calculated from the data is also shown in this figure.

Correlations between hemispheres came from both geometrical and kinematic effects, as described in section 4.4. The hemisphere correlation in b events for this analysis was estimated from the simulation to be

$$\rho_b = (0.87 \pm 0.30(\text{stat}) \pm 0.21(\text{syst})) \times 10^{-2}. \tag{18}$$

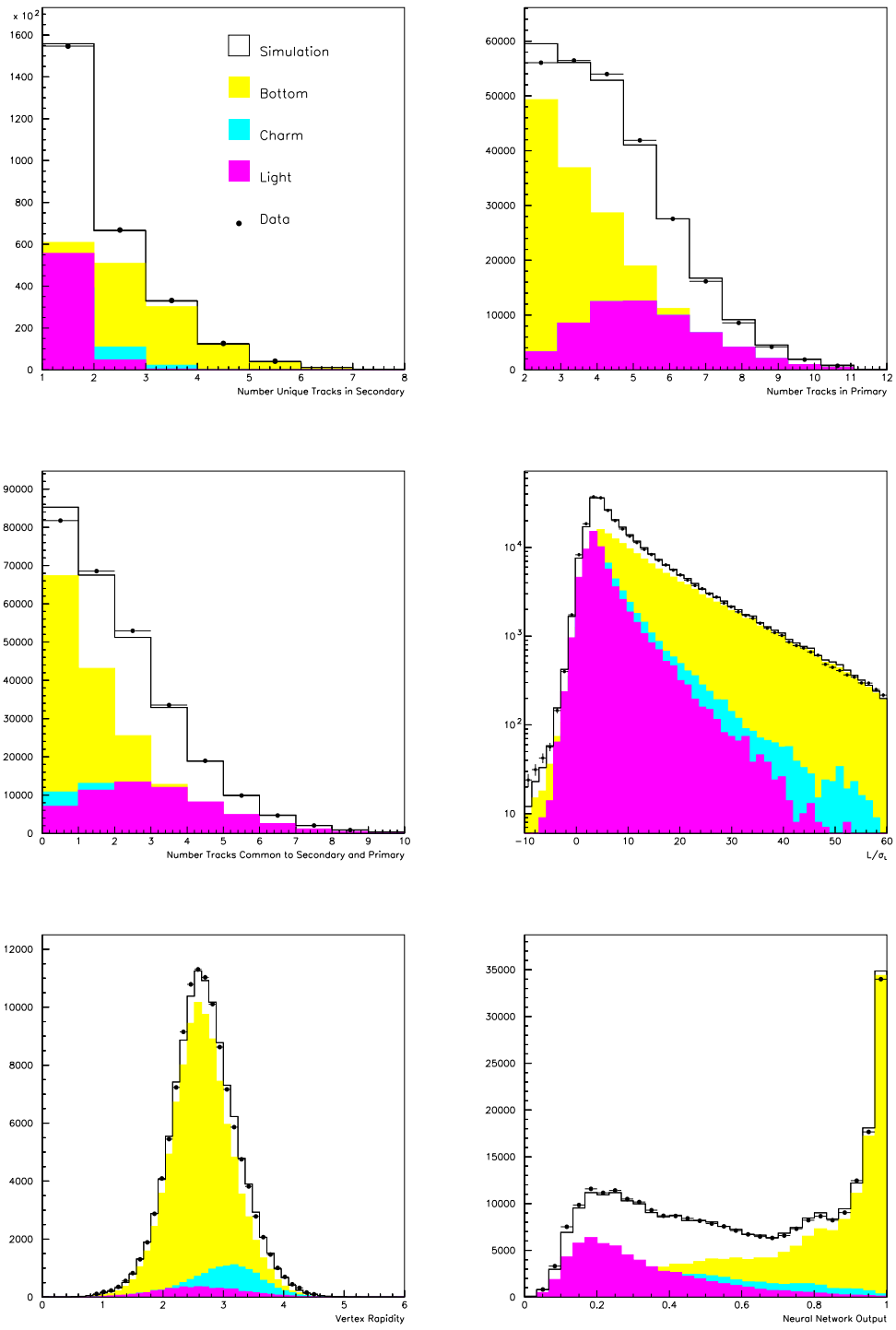

Figure 13: Comparison of data and simulation distributions of the 5 input variables to the neural network and of the single output.

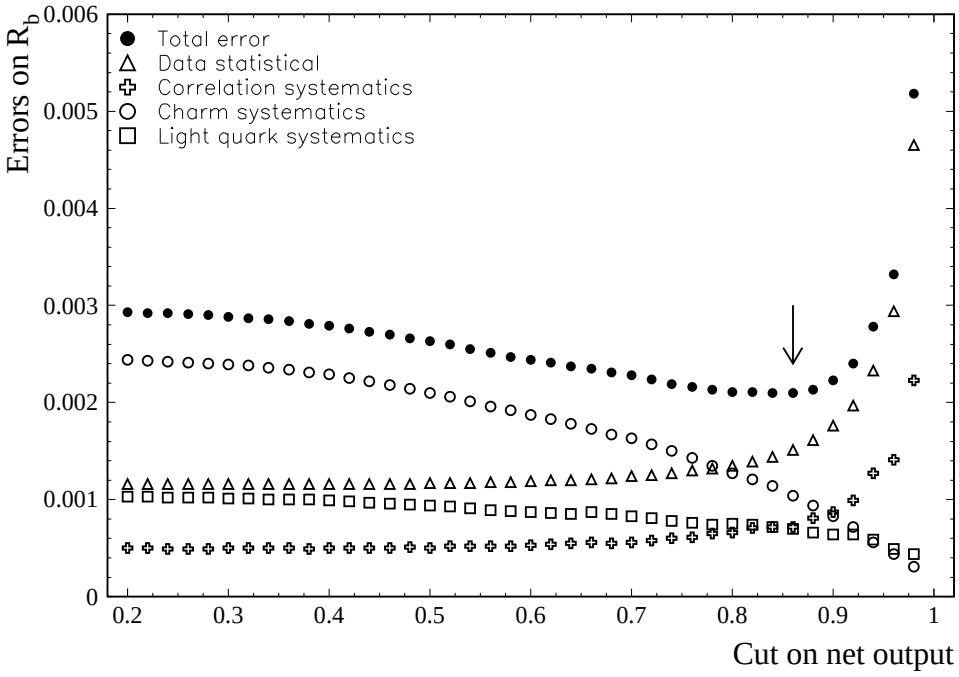

Figure 14: Contributions to the error on R_b. The arrow marks the position of the cut.

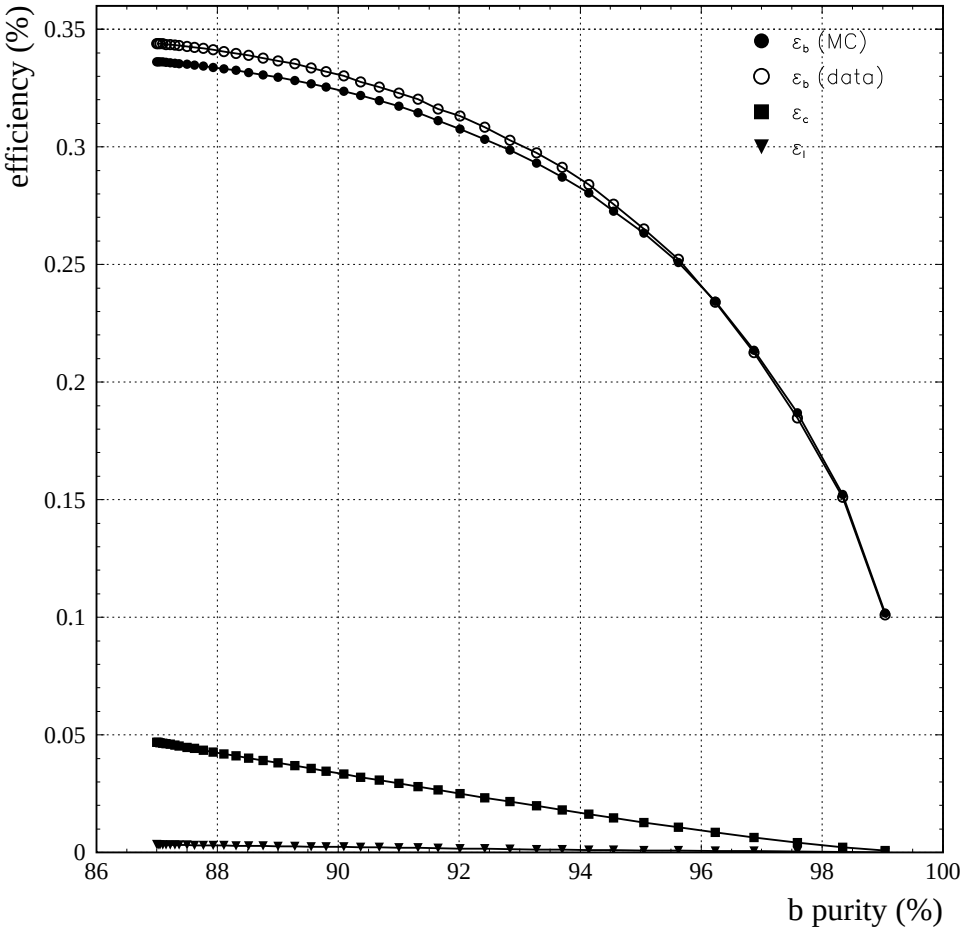

Figure 15: The efficiencies for tagging different quark flavours as a function of the b purity taken from the simulation. The good agreement between the efficiency for tagging b hemispheres extracted from the simulation and that measured in the data is shown.

The first error is due to the limited simulation statistics and the second is the estimated systematic effect. Contributions to the systematic error from both geometrical effects and physics modelling are estimated as described in section 4.4 and are summarized in table 12. This analysis made use of a primary vertex determination, based only on tracks within a hemisphere, for the secondary vertex search and a run-averaged beamspot for the decay length calculation. It was found that these choices had a negligible effect on the calculated correlation.

7.4 Results

Using the numbers of hemispheres and events tagged in the data and the values for the efficiencies and correlations given above, and taking into account the selection bias towards $Z \to b\bar{b}$ events, R_b was calculated to be:

$$R_b = 0.2154 \pm 0.0014(\text{stat}) \pm 0.0015(\text{syst}) - 0.087 \times (R_c - 0.172). \tag{19}$$

The b-tagging efficiency calculated simultaneously from the data was $(26.5 \pm 0.2)\%$, compared to 26.3% in the simulation. The stability of the measurement over a range of b purities can be seen in figure 16.

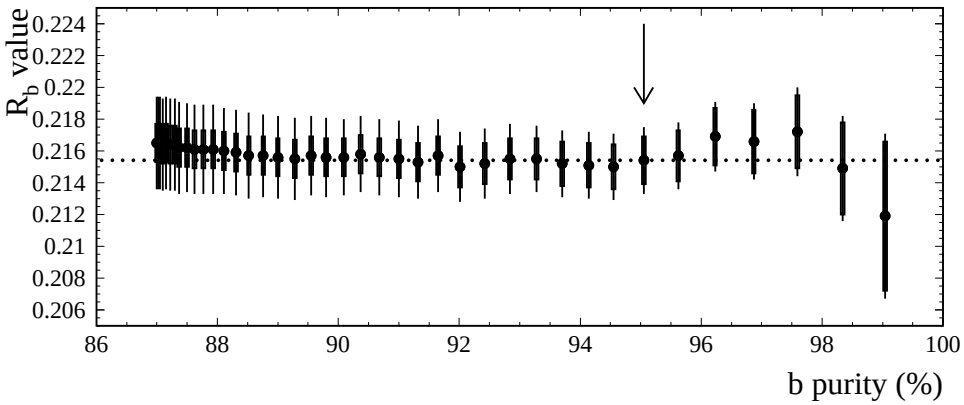

Figure 16: The measured value of R_b as a function of the b purity taken from the simulation. The thick error bars show the statistical errors, the thinner bars indicate the total errors, and all errors are correlated from point to point. The arrow marks the position of the cut and the line shows the value at the chosen cut.

A full breakdown of the systematic error contributions on R_b is shown in table 12.

Error Source	Range	$\Delta R_b \times 10^4$ vert
Internal experimental effects:		
Hemisphere correlations		$\pm$ 7.7
Detector effects		$\pm$ 3.6
Acceptance bias		$\pm$ 1.9
$\langle x_E(\mathrm{b})\rangle$	0.702 $\pm$ 0.008	$\mp$ 2.6
$\langle x_E(\mathrm{c})\rangle$	0.484 $\pm$ 0.008	$\mp$ 1.7
D^0 lifetime	0.415 $\pm$ 0.004 ps	$\mp$ 1.0
D^+ lifetime	1.057 $\pm$ 0.015 ps	$\mp$ 0.7
$\mathrm{D_s}$ lifetime	0.467 $\pm$ 0.017 ps	$\mp$ 0.9
Λ_c lifetime	0.206 $\pm$ 0.012 ps	$\mp$ 0.8
B lifetime	1.55 $\pm$ 0.05 ps	$\mp$ 0.1
B decay multiplicity	5.73 $\pm$ 0.35	$\pm$ 1.1
D decay multiplicity	2.39 $\pm$ 0.14	$\mp$ 4.7
$BR(D \to K^0 X)$	0.46 $\pm$ 0.06	$\pm$ 5.8
$g \to \mathrm{c\bar{c}}$	(2.38 $\pm$ 0.48)%	$\mp$ 4.2
$g \to \mathrm{b\bar{b}}$	(0.13 $\pm$ 0.04) $\times(g \to \mathrm{c\bar{c}})$	$\mp$ 3.9
Light hadron modelling	tuned JETSET $\pm$ 10%	$\mp$ 2.2
QCD hemisphere correlations	see text	$\pm$ 2.4
D^+ fraction	0.231 $\pm$ 0.026	$\mp$ 4.4
$\mathrm{D_s}$ fraction	0.110 $\pm$ 0.017	$\mp$ 0.5
c-baryon fraction	0.063 $\pm$ 0.029	$\pm$ 2.9

Table 12: Summary of systematic errors on R_b from the secondary vertex analysis on 1994 data. Details concerning the different error sources can be found in [17].

8 Conclusions

Three different measurements of the partial decay width R_b^0 of the Z into B-hadrons have been performed. Events were selected using either tracks having large impact parameters in jets with reconstructed secondary vertices or with a multivariate technique or with a neural network. The following results were obtained.
Double impact parameter tag (1994 data):

$$R_b = 0.21697 \pm 0.00119(stat.) \pm 0.00096(syst.) - 0.033 \times (R_c - 0.172),$$

Multivariate analysis (1994 and 1995 data):

$$R_b = 0.21640 \pm 0.00082(stat.) \pm 0.00088(syst.) - 0.024 \times (R_c - 0.172).$$

Secondary vertices (1994 data):

$$R_b = 0.2154 \pm 0.0014(stat.) \pm 0.0015(syst.) - 0.087 \times (R_c - 0.172).$$

The third analysis is not combined with the others since the statistical correlation has still to be computed.

The multivariate analysis relies heavily on the impact parameter combined analysis, which acts as the tight b-tag. The results are therefore highly correlated between each other, and cannot be used independently. Since they are statistically consistent the analysis with the smallest total error (the multivariate analysis) is taken as the result. Applying the small (0.00020) correction for photon exchange yields for the ratio of partial widths:

$$R_b^0 = 0.21660 \pm 0.00082(stat.) \pm 0.00088(syst.) - 0.024 \times (R_c - 0.172).$$

For this number, all centre of mass energies at which LEP has run have been combined. All results are in agreement with those of other measurements at LEP [1, 2, 4, 5, 6]. The result is in good agreement with the Standard Model expectation of $R_b^0 = 0.2158 \mp 0.0005$ [26], assuming a mass of the top quark of $m_t = 175.6 \pm 5.5\ GeV/c^2$ [28].

Acknowledgements

We are greatly indebted to our technical collaborators and to the funding agencies for their support in building and operating the DELPHI detector, and to the members of the CERN-SL Division for the excellent performance of the LEP collider.

References

[1] ALEPH Collaboration, R.Barate et al., Phys. Lett.**B401** (1997) 150.

[2] ALEPH Collaboration., D. Barate et al., Phys. Lett. **B401** (1997) 163.

[3] DELPHI Collaboration, P. Abreu et al., Z. Phys. **C70** (1996) 531.
DELPHI Collaboration, P. Abreu et al., Z. Phys. **C66** (1995) 323.

[4] L3 Collaboration, O. Adriani et al., Phys. Lett. **B307** (1993) 237.

[5] OPAL Collaboration, K.Ackerstaff et al., Z. Phys. **C74** (1997) 1.

[6] SLD Collaboration, SLAC-PUB-7481 (to be submitted to Phys. Rev. Lett.)

[7] The LEP Collaboration and SLD, *A Combination of Preliminary Electroweak Measurements and Constraints on the Standard Model*, CERN-PPE/96-183.

[8] DELPHI Collaboration, P. Aarnio et al., Nucl. Inst. Meth. **A303** (1991) 233.

[9] DELPHI Collaboration, P. Abreu et al., Nucl. Inst. Meth. **A378** (1996) 57.

[10] N. Bingefors et al., Nucl. Inst. Meth. **A328** (1993) 447.

[11] V. Chabaud et al., Nucl. Inst. Meth **A368** (1996) 314.

[12] T. Sjöstrand et al., in *"Z physics at LEP 1"*, CERN 89-08, CERN, Geneva, 1989;
Comp. Phys. Comm. **39** (1986) 347.

[13] G. Borisov and C. Mariotti, *Fine Tuning of Track Impact Parameter Resolution of the DELPHI Detector*, Nucl. Inst. Meth. **A372** 181.
G. Borisov and C. Mariotti, *Tuning of the Track Impact Parameter Resolution of the Upgraded DELPHI Detector*, DELPHI note, DELPHI 97-95 PHYS 717.

[14] G. Borisov, *Combined b-tagging*, DELPHI note, DELPHI 97-94 PHYS 716.

[15] ALEPH Collaboration, D. Buskulic et al., Phys. Lett. **B313** (1993), 535.

[16] G.V.Borisov, *Lifetime Tag of Events with B-hadrons with the DELPHI Detector*, preprint IHEP (Protvino), 94-98 (1994).

[17] The LEP Collaborations Nucl. Inst. Meth. A378 (1996) 101;
The LEP Heavy Flavour Working Group , *Presentation of LEP Electroweak Heavy Flavour Result for Summer 1996 Conferences*, LEPHF 96-01.

[18] C. Mariotti, *New measurement of the charged particle multiplicity of weakly decay B hadrons with the DELPHI detector at LEP*, DELPHI 97-125 CONF 106, submitted to HEP'97 Conference in Jerusalem.

[19] A.G. Frodesen, O. Skeggestad and H. Tofte, *Probability and statistics in particle physics*, Universitetsforlaget 1979.

[20] NAGLIB Manual. CERN Program Library.

[21] P. Billoir et al., Nucl. Inst. Meth. **A360** (1995) 532.

[22] Ch. De la Vaissière and F. Martínez-Vidal, *Description and Performances of the DELPHI multivariate flavour tagging*, DELPHI 97-134 PHYS 721.

[23] W.J. Murray, *Improved B tagging using impact parameters*, internal DELPHI Note, DELPHI 95-167 PHYS 581.

[24] F. Caravaglios and G. Ross, Phys. Lett. **B346** (1995) 159.

[25] P. Kluit, *A measurement of the cross sections and asymmetries for flavour tagged events at energies of 161 and 172 GeV and limits on new interactions*, DELPHI 97-93 CONF 78, submitted to HEP'97 Conference in Jerusalem.

[26] D. Bardine et al., *ZFITTER: An Analytical Program for Fermion Pair Production in e^+e^- Annihilation*, CERN-TH 6443/92 (May 1992).

[27] A. Zell et al., *Stuttgart Neural Network Simulator*, University of Stuttgart, Institute for Parallel and Distributed High Performance Systems.

[28] CDF Collaboration, J. Lys, Proceedings ICHEP'96, Warsaw (1996), and FERMILAB-CONF-96/409-E;
D0 Collaboration, E.W.Warnes, Proceedings ICHEP'96, Warsaw (1996), and FERMILAB-CONF-96/243-E.